CH_4 and N_2O fluctuations during the penultimate deglaciation

Loïc Schmidely[1], Christoph Nehrbass-Ahles[2], Jochen Schmitt[1], Juhyeong Han[1], Lucas Silva[1], Jinwha Shin[3,a], Fortunat Joos[1], Jérôme Chappellaz[3], Hubertus Fischer[1], and Thomas F. Stocker[1]

[1]Climate and Environmental Physics, Physics Institute and Oeschger Centre for Climate Change Research, University of Bern, Bern 3012, Switzerland
[2]Department of Earth Sciences, University of Cambridge, Cambridge, UK
[3]CNRS, Univ. Grenoble-Alpes, Institut des Géosciences de l'Environnement (IGE), Grenoble, France
[a]Present address: Department of Earth and Atmospheric Sciences, University of Alberta, Edmonton, AB, T6G 2E3, Canada

Correspondence: Thomas Stocker (thomas.stocker@climate.unibe.ch)

Abstract. Deglaciations are characterized by the largest natural changes in methane (CH_4) and nitrous oxide (N_2O) concentrations of the past 800 thousand years. Reconstructions of millennial to centennial-scale variability within these periods are mostly restricted to the last deglaciation. In this study, we present composite records of CH_4 and N_2O concentrations from the EPICA Dome C ice core covering the penultimate deglaciation at temporal resolutions of ~100 years. Our data permit the identification of centennial-scale fluctuations ~~standing out of the overall transition~~ during the transition from glacial to interglacial levels. ~~These features occurred in concert with reinvigorations of the Atlantic Meridional Overturning Circulation (AMOC) and northward shifts of the Intertropical Convergence Zone. The abrupt CH_4 and N_2O rises at~~ At ~134 and ~~128 thousand of~~ 129 thousand years before present (hereafter ka BP)~~are assimilated~~ , both CH_4 and N_2O increased on centennial-timescales. These abrupt rises are similar to the fluctuations ~~accompanying~~ associated with the Dansgaard–Oeschger events ~~of~~ identified in the last glacial period~~, while~~ . In addition, gradually rising N_2O levels at ~~130.5 ka BP are assimilated to~~ 130 ka BP resemble a pattern of increasing N_2O concentrations ~~that characterized the end~~ on millennial-time scales characterizing the later part of Heinrich stadials. ~~We suggest the 130.5-ka event to be driven by a partial reinvigoration of the AMOC.~~ Overall, the events in CH_4 and N_2O ~~fluctuations~~ during the penultimate deglaciation exhibit modes of variability that are also found during the last deglaciation ~~. However, trace gas responses may differ for similar type of climatic events, as exemplified by the reduced amplitude and duration of the 134-ka event compared to the fluctuations of the Bølling–Allerød during the last deglaciation~~and glacial cycle, suggesting that the processes leading to changes in emission during the transitions were similar but their timing differed.

1 Introduction

Methane (CH_4) and nitrous oxide (N_2O) are currently the second and third most potent well-mixed ~~gases in terms of radiative forcing (0.48 ± 0.05 Wm^{-2} and 0.17 ± 0.03 Wm^{-2}, respectively)~~ anthropogenic greenhouse gases after carbon dioxide (CO_2) (Myhre et al., 2013). The impact of these trace gases on the Earth's radiative balance in the future depends ~~also~~ on the sensitivity of natural sources to anthropogenic warming. Time periods of climate change in the past provide natural templates to study this coupling (Fischer et al., 2018). Reconstructions of ~~trace~~ greenhouse gas concentrations before the

instrumental era are only enabled by analyzing the composition of air trapped in tiny bubbles in polar ice cores, reflecting the atmospheric composition at the time the bubbles were formed. Ice core records of CH_4 and N_2O concentrations combined with temperature reconstructions ~~documented~~ revealed the natural variability of ~~the trace~~ these gases and their coupling to climate change during the glacial cycles of the past 800 thousand years. The overall increase in concentrations accompanying deglaciations ~~represent~~ represents the largest recurring changes (Spahni et al., 2005; Loulergue et al., 2008; Schilt et al., 2010a). Records spanning the last deglaciation (Termination I (TI), 18–11 thousand ~~of~~ years before present (hereafter ka BP), where ~~*present*~~ present is defined as 1950 Common Era) showed that this overall increase appears as a sequence of millennial and centennial fluctuations ~~superposed~~superimposed, for CH_4, on longer-term gradually rising concentrations ~~(Marcott et al., 2014; Rhodes et al., 2015; Fischer et al., 2019)~~(Marcott et al., 2014; Rhodes et al., 2015). Records resolving short-term fluctuations within deglaciations are limited to TI, owing to the availability of multiple high-accumulation ice cores.

The aim of this study is to ~~extend the deglacial record to~~ produce a high-resolution deglacial record for the penultimate deglaciation (Termination II (TII), 140–128 ka BP). We present ~~high-resolution~~ CH_4 and N_2O composite datasets from the EPICA Dome C (EDC) ice core including 150 new measurements covering the time interval ~~from~~ 145–125 ka BP, combined with the published data of Loulergue et al. (2008) and Schilt et al. (2010a). We increased the sampling ~~density~~ resolution of the aforementioned records by a factor ∼3.5 and ∼5 to obtain mean resolutions of 100 and 115 years for CH_4 and N_2O, respectively~~,~~. These values are on the order of the mean width of the gas age distribution (GAD) ~~at EDC (estimated at~~ for the EDC ice core in the interval 145-125 ka BP. This width is estimated to range between ∼~~170 years for TII~~ 110–220 years using the approach of Nehrbass-Ahles et al. (2020)~~)~~, where the width is defined as the arithmetic mean of the distribution) and ∼50–130 years using the approach of Epifanio et al. (2020), where the width is defined as the spectral width of the distribution. In addition, we ~~present a coarse resolution record of~~ also present 7 N_2O isotopic ~~composition~~ measurements ($\delta^{15}N(N_2O)$ and $\delta^{18}O(N_2O)$), used to assess the integrity of the data with respect to in situ formation of N_2O~~measurements. Overall, our data allow us to study the extent to which the evolution of~~ .

CH_4 and N_2O ~~concentrations differ between the last two deglaciations.~~

~~Millennial fluctuations observed within~~ fluctuations observed during TI belong to ~~a mode of variability,~~ recurrent modes of variability. The most studied of these modes characterizes the climate transitions from stadials to interstadials, and is most notably exemplified ~~in the frame of the Dansgaard–Oeschger~~ by the transitions associated with the Dansgaard-Oeschger (DO) events of the last glacial ~~, where CH_4 and N_2O concentrations respond to Greenland temperature fluctuations. The DO-like~~ period as well as by the transitions to the Bølling-Allerød and the Holocene during TI. This *DO-type* mode of variability is characterized by abrupt increases in CH_4 concentrations (∼50–260 ppb in a few centuries), ~~synchronous or slightly lagging~~ approximately synchronous with the onsets of interstadial Greenland warming by a few decades ~~(Baumgartner et al., 2014; Huber et al., 200~~ (Baumgartner et al., 2014; Rosen et al., 2014), while N_2O concentrations exhibit concomitant ~~fluctuations~~ increases reaching up to ∼60 ppb, taking more than a century to stabilize because of its longer atmospheric lifetime (Flückiger et al., 2004; Schilt et al., 2010a, 2013). In addition, ~~particularly low~~ N_2O concentrations are ~~observed during~~ gradually increasing in the later part of Heinrich stadials (HS), extended stadials defined by the occurrence of massive iceberg discharges through the Hudson Strait

into the North-Atlantic (Hemming, 2004). At the end of the HS, N_2O concentrations start increasing , starting centuries to millennia before the interstadial Greenland temperature and CH_4 rises (Schilt et al., 2013)(*Late stadial* increase). This mode of variability has been evidenced for . This *late HS-type* mode of N_2O variability characterized the HS during the last both the last deglaciation (Fischer et al., 2019; Schilt et al., 2014) as well as the last glacial period (Schilt et al., 2013)and the last deglaciation (Fischer et al., 2019; Schilt et al., 2014).

The centennial CH. A second mode of CH_4 variability has been identified during HS of the last glacial and deglaciation. This *HS-type* mode of CH_4 fluctuations within TI belong to a mode of variability found in HS 1,2,4 and 5 (*Intra-stadial* variability). This pattern consists of short-lived increases reaching amplitudes of ~30–55 variability consists of intermittent CH_4 peaks displaying amplitudes of 32–53 ppb and characteristic timescales of ~100–300 years, associated with large iceberg discharges in the North-Atlantic 90–190 years, sometimes followed (HS4 and HS5) by elevated background concentrations relative to before the event (Rhodes et al., 2015).

DO-like and intra-stadial DO-type and HS-type CH_4 fluctuations are likely driven by changes in tropical wetland emissions (Rhodes et al., 2015; Bock et al., 2017), where CH_4 is produced by the decomposition of organic matter under anaerobic conditions. Changes in geologic and pyrogenic emissions as well as changes in the sink strength play only a minor role (Dyonisius et al., 2020; Bock et al., 2010, 2017; Levine et al., 2012; Hopcroft et al., 2017). Wetland emissions are controlled by climate (precipitation, temperature, and atmospheric CO_2 concentration), modulating wetland extent, emission rates, and ecosystem composition (Van Groenigen et al., 2011; Melton et al., 2013; Bloom et al., 2010). Changes in tropical wetland emissions during DO-like events DO-type fluctuations are linked to the strengthening of monsoonal precipitation in the Northern Hemisphere (NH) tropics, enhancing wetland emission rates (Bock et al., 2017). Increased NH tropical precipitation is associated to northward shifts of the Intertropical Convergence Zone (ITCZ) in response to changes in heat distribution by the Atlantic Meridional Overturning Circulation (AMOC) (Broccoli et al., 2006; Alley, 2007). On the other hand, intra-stadial fluctuations are believed HS-type CH_4 fluctuations are hypothesized to result from southward shifts large iceberg discharges, associated with a southward shift of the ITCZ, strengthening leading to an intensification of monsoonal precipitation in the Southern Hemisphere (SH) tropics, leading to ultimately producing an increase in wetland emissions there (Rhodes et al., 2015).

DO-like DO-type N_2O variability is likely driven by changes in emission from the terrestrial and marine biospheres, where N_2O is emitted as a by-product of nitrification and intermediate product of denitrification (Joos et al., 2019, 2020; Fischer et al., 2019; Schilt et al., 2014). Terrestrial emissions are controlled by climate (precipitation, temperature, and atmospheric CO_2 concentration) and available land area (Joos et al., 2020; Van Groenigen et al., 2011). During TI, the response of terrestrial sources to DO-like N_2O emissions for DO-type fluctuations is believed to result from temperature and precipitation changes (Joos et al., 2020), appeared in phase with Greenland warming , and lasted with the transition period lasting maximum ~200 years (Fischer et al., 2019). Marine emissions are linked to the strength of the AMOC, modulating oxygen concentrations in the upper ocean and the amount of organic matter converted into minerals available organic matter at depth. During DO-like eventsFor DO-type fluctuations, marine emissions are believed to be stimulated mainly by deoxygenation in the upper ocean as a consequence of the reinvigoration of the AMOC (Joos et al., 2019). Finally, the late stadial HS-type N_2O increases increase during TI is thought to be driven exclusively by marine emissions (Fischer et al., 2019; Schilt et al., 2014), maybe possibly

resulting from a long-term reorganization of the nitrate and oxygen ~~concentrations~~ inventories following the preceding AMOC collapse (Schmittner and Galbraith, 2008).

2 ~~Methods~~Method

The results presented in this study are derived from two different instruments. The $\delta^{15}N(N_2O)$ and $\delta^{18}O(N_2O)$ data were measured with the device described in Schmitt et al. (2014), ~~while~~ combining continuous extraction under vacuum with gas chromatography (GC) and isotope ratio mass spectrometry.

CH_4 and N_2O ~~concentrations~~ measurements were performed with a ~~newly developed~~ completely revised analytical system, firstly ~~deployed for this measurement campaign. In the following, we present this new system with an emphasis on the major differences compared to the previous version of the instrument used at the University of Bern.~~

~~Our new measurement system combines a custom-made extraction unit with a gas chromatograph (GC) equipped with a thermal conductivity detector (air), a flame-ionization detector (~~employed during this study (comprehensive description in Appendix A). The new apparatus uses continuous extraction under vacuum, comparable to the approach of Schmitt et al. (2014) or Oyabu et al. (2020), combined with GC techniques to determine CH_4 ~~) and an electron capture detector (~~and N_2O ~~). The system is optimized for the measurement of small amount of analytes, enabling to use as little as~~ mole fractions in air extracted from small (~20 g~~of EDC ice core samples . The major modifications compared to the previous version of the instrument are the change from a melt-refreeze extraction method (e.g. Flückiger et al., 1999, 2002, 2004; Spahni et al., 2005; Schilt et al., 2010a, b; Baumga to a continuous extraction under vacuum, according to the procedure described in Schmitt et al. (2014), as well as the complete renewal of the standardization procedure.~~

~~In our extraction unit, air released from the ice during the melting phase (immersion in a water bath at ~293 K) is continuously adsorbed on an activated charcoal trap held at 77 K using liquid nitrogen. This extraction technique ensures low CH_4 and N_2O partial pressures above the meltwater, minimizing dissolution during the melting, thereby avoiding the need for a refreezing step. To calibrate our measurements, we use a set of three standard gases provided by the National Oceanic and Atmospheric Administration, covering the typical glacial-interglacial concentration range for~~) ice samples with a sample throughput of 5-6 samples per day. The instrument is equipped with a thermal conductivity detector, a flame-ionization detector and an electron-capture detector for the quantification of air. CH_4 ~~(358.88 ± 0.16 ppb, 838.59 ± 0.28 ppb, and 1729.30 ± 0.34 ppb) and~~ and N_2O~~(187.10 ± 0.12 ppb, 194.13 ± 0.12 ppb, and 300.20 ± 0.12 ppb). The standards~~ , respectively. The results are referenced to the World Meteorological Organisation mole fraction scales: WMOX2004A scale (CH_4) and NOAA-2006A (N_2O) (Dlugokencky et al., 2005; Hall et al., 2007) ~~.~~

~~To increase the sample throughput, standard gases are injected directly into the GC system, bypassing the extraction line employed for ice core samples. We periodically inject standards over gas-free ice samples to account for contamination along the extraction line, determined as the mean offset between the two injection pathways (line offset). For~~ using three standard gases bracketing the glacial-interglacial range of CH_4 ~~, the line offset depends linearly on concentrations (R^2 = 0.99) leading~~

to a downward revision of our measured values by up to 5 ppb(for concentrations ranging between 350 and 700 pbb). For N_2O, the line offset is constant and leads to a downward revision of the measured values by 4 ppb.

The construction of composite records is complicated by offsets between the datasets, where our results appear 29 (358.88±7 ppb(CH_4) and 18 0.16 ppb, 838.59±2 ppb (0.28 ppb, and 1729.30±0.34 ppb) and N_2O) higher than previous data. The offset is calculated as the mean of the residuals between splines with cut-off periods of 10 thousand years fitted through the datasets. We computed splines according to Enting (1987), using the same routine as Beck et al. (2018), where each spline is the average of 1000 iterations with data points varied within a normal distribution inside their 1σ uncertainty range. Because we are unable to experimentally compare the accuracy of different instruments using different extraction procedures, we adopt an *ad hoc* approach and subtract 29 concentrations (187.10±7 ppband 18 0.12 ppb, 194.13±2 ppbfrom our new CH_4 and N_2O results, respectively, to reach consistency with the datasets of Loulergue et al. (2008) and Schilt et al. (2010a). For the same reason, we do not correct for gravitational and thermal fractionation in the firn.

The precision of our new data amounts to 10 ppb for CH_4 0.12 ppb, and 6 ppb for N_2O and is calculated as the square-root of the sum in quadrature of the individual uncertainties associated with the analytical procedure, the line offset correction and the inter-dataset correction. The analytical part corresponds to the standard deviation (1σ)of standards injected over gas-free ice samples300.20±0.12 ppb). The uncertainty of the line offset correction corresponds to the standard deviation (1σ) of the mean offset between the two injection pathways (as described above). The uncertainty of the inter-dataset correction is the standard deviation (1σ) of the mean residuals between the splines. For the existing EDC data and the isotopic measurements , the precision amounts to 10 measurements derived from the revised instrument amounts to 7 ppb (CH_4) , 4 and 6 ppb (N_2O), 0.22 ‰ ($\delta^{15}N(N_2O)$), and 0.34 ‰ ($\delta^{18}O(N_2O)$) (Loulergue et al., 2008; Schilt et al., 2010a; Schmitt et al., 2014).

3 Results

Our centennial-scale records show the progressions of the overall ∼370 390 ppb and ∼60 ppb increase in CH_4 and N_2O concentration (Fig. 1), respectively, over the penultimate deglaciation (Fig. **??**) from the end of the Penultimate Glacial Maximum (PGM) to the beginning of the Last Interglacial (LIG). Our CH_4 data identifies an outlier at 139.9 outstanding value at ∼140 ka BP, in the dataset by Loulergue et al. (2008), ∼80 ppb higher than adjacent samples . (Fig. 1). The N_2O data appear substantially more scattered in the early part of the record, especially around the penultimate glacial maximum (∼145–140 ka BP), where several high-amplitude spikes reach up to ∼300 ppb. This scatter tends to decrease with younger ages. The spikes appear in the interval where the isotopic composition of N_2O becomes enriched in $\delta^{15}N(N_2O)$ (up to 21 ‰) and depleted in $\delta^{18}O(N_2O)$ (down to 41 ‰), compared to the relatively steady values in the range of ∼11–14 ‰ and ∼45–47 ‰, respectively, observed for 125–136 ka BP (Fig. **??**1).

Our records display several fluctuations standing out in the overall evolution of the CH_4 and N_2O concentrations(Fig. **??**). For CH_4, we distinguish between periods of relatively gradual increase and periods marked by more abrupt fluctuations based on mean these events are identified based on their high rates of change observed in the ice core record over the corresponding time period. Abrupt (>10 ppb per century, Table 1). CH_4 rises are identified on centennial-timescales at ∼134 and ∼128 129

ka BP. ~~The 134-ka event exhibits an increase at a mean rate of 34 ppb per century, in the interval from~~ At ~~134.0 to 133.8~~ 134 ka BP, ~~and a decrease at a mean rate of 23 ppb per century, in the interval from~~ concentrations increased by ~~133.8 to 133.6 ka BP. During the rising limb, concentrations increase from~~ 70 ppb in ~~440 ppb to~~ 200 years before declining by ~~510 ppb before declining back to~~ 60 ppb in ~~460 ppb . The 128-ka~~ 400 years. The 129-ka event consists of a ~~190 ppb increase (from ~530 to 720 ppb, about half of the deglacial change)~~ 200 ppb increase proceeding in ~300 years~~(~128.9–128.6 ka BP). This feature exhibits the highest mean growth rate observed in our deglacial CH_4 record (mean of 61 ppb per century). Beside the 134 and 128-ka events, CH_4 was also released relatively fast during the initial deglacial rise (~139.6–138.7 ka BP, mean of 7 ppb per century) compared to the other time periods of more gradual increases (mean of 3 ppb per century from ~135.6 to 134.0 ka BP and from ~132.0 to 128.9 ka BP). However, the mean growth rate at this time is still well below those of the abrupt fluctuations.~~ .

The evolution of N_2O concentrations alternates between periods of plateaus and well-marked fluctuations~~(Fig. ??).~~ . Similar to CH_4, a feature is resolved at ~134 ka BP ~~, exhibiting the highest rate of change observed in our deglacial N_2O record (mean of 12 ppb per century during the rising limb). Concentrations increased~~ where concentrations increased by ~30 ppb in ~~200 years (134–133.8 ka BP) from~~ 300 years before declining to previous levels in ~~210 to 240 ppb before stabilizing for ~200 years and declining from ~133.6 ka BP onwards. The decay phase lasted for ~~1000 ~~year (~133.6–132.6 ka BP) at a mean rate of 3 ppb per century. The 128-ka~~ years. The 129-ka event is also imprinted in our N_2O record ~~(~129.0–128.2 ka BP)~~ and is characterized by ~~rising concentrations from~~ a ~~240 to~~ 30 ppb rise in ~~270 ppb at a mean growth rate of 3 ppb per century~~900 years. In addition, an increase is identified at ~~130.5 ka BP(~130.5–129.8 ka BP)~~130 ka BP, where concentrations rose ~~from~~ by ~~220 to 245 ppb at a mean growth rate of 3 ppb per century. The 130.5-ka and 128-ka~~ 20 ppb in ~700 years. The 130-ka and 129-ka events are separated by a plateau that lasted ~~800~~ ~1000 years.

Overall, the improved resolution of our records allowed us to identify features ~~hidden in the current~~ not resolved in the previously published CH_4 and N_2O EDC datasets. In particular, the 134-ka event and the 130-ka event in N_2O ~~increase at ~130.5 ka BP~~ are resolved for the first time. Retrieving CH_4 and N_2O concentrations from the same samples enable us to study the relative phasing of both trace gases in the course of these events without age uncertainty. At the onset of the 134 and ~~128-ka~~ 129-ka events, the rise in both trace gases occur simultaneously. In contrast, the ~~130.5-ka~~ 130-ka event in the N_2O record is not accompanied by a concomitant fluctuation in CH_4 concentrations.

4 Discussion

4.1 Non-atmospheric CH_4 and N_2O variability

Interpreting our records in terms of atmospheric variability requires a closer inspection of the extreme values observed in the CH_4 and N_2O records.

The CH_4 data point at ~~139.9 ka BP~~~140 ka BP, previously published by Loulergue et al. (2008), is measured in the section characterized by the widest GAD in our record. ~~Using the tentative approach of Nehrbass-Ahles et al. (2020) yields a mean~~ For the time interval 141-139 ka BP, the width of the GAD ~~estimated at~~ is on the order of ~220 years~~for the interval from 139 to~~

141 ka BP. The , using the approach of Nehrbass-Ahles et al. (2020), or ∼120 years using the approach of Epifanio et al. (2020) . At ∼140 ka BP, the adjacent data points are ∼160 years older and 173 ∼170 years younger than the extreme measurement, i. e., the timescale of the hypothetic fluctuation at 139.9 ka BP is smaller than the GAD. This feature is therefore unlikely to represent atmospheric variability and has to be considered as an outlier, likely resulting from the analytical procedure. Such signals may also data point in question. Consequently, it appears unlikely that such an abrupt fluctuation in the ice core record represents an atmospheric signal. Spurious peaks could potentially result from layered bubble trapping (Rhodes et al., 2016; Fourteau et al., 2017, 2020). However, the this outlier is measured in a period of otherwise stable CH_4 concentrations, where neither early nor late pore closures are expected to generate an anomaly (Rhodes et al., 2016; Fourteau et al., 2017). Secondly, similarly high concentrations are not observed in our record before the 134-ka event. This would imply Such an age anomaly (between the layers enclosing gas of abnormal age and the layers enclosing gas of the corresponding age) that is expected age) would be unrealistically high compared to the characteristic age anomaly anomalies reported by Fourteau et al. (2017) for the Vostok ice core (∼200 years). Accordingly, we regard this measurement as an analytical outlierat this point and exclude it from further analysisconsider this CH_4 data point as an outlier.

The large variability observed in adjacent data points during the early part of the N_2O record (Fig. **??**1) is unlikely to reflect atmospheric fluctuations given the its atmospheric lifetime of N_2O of 116 ± 9 years (Prather et al., 2015). Elevated concentrations and disproportionately high N_2O variability have been observed in many instances for ice samples rich in mineral dust in both Antarctic and Greenland ice cores and are attributed to in situ production (Flückiger et al., 1999; Sowers, 2001; Flückiger et al., 2004; Spahni et al., 2005; Schilt et al., 2010a, 2013; Fischer et al., 2019). Measurements in the Vostok ice core by Sowers (2001) demonstrated this excess N_2O production to have a strong imprint on in both $\delta^{15}N(N_2O)$ and $\delta^{18}O(N_2O)$ records. For some of our EDC samples we observe the same systematic isotopic deviations as for the Vostok samples of that period, with $\delta^{15}N(N_2O)$ and $\delta^{18}O(N_2O)$ values that are heavier and lighterenriched and depleted, respectively, than the typical atmospheric valuetypical atmospheric values. The coupling with dust is the basis of an empirical artifact detection method , applicable to EDC samples, considering measurements for . This method considers depth intervals where dust concentrations exceed an arbitrary threshold of 300 μg kg^{-1} as affected by in situ production (Spahni et al., 2005; Schilt et al., 2010a). We follow this approach and define 134.5 ka BP , as the boundary for the section affected by artifacts. This is a slightly younger age than the last value considered as unbiased by Schilt et al. (2010a), as the boundary for the section affected by artifacts. In summary. Consequently, we refrain from interpreting N_2O data points older than 134.5 ka BP as reflecting atmospheric variability.

The younger part of our records are used to study the nature of the CH_4 and N_2O fluctuations during TIIand to compare with TI (Fig. **??**). For such comparisons, we take the WAIS Divide ice core record (WD) (Rhodes et al., 2015) and the composite dataset of Fischer et al. (2019) as benchmarks for CH_4 and N_2O concentrations, respectively, in the last deglaciation. The nature of the fluctuations is assessed by analyzing the amplitude and timescale of the individual features . In particular, we scrutinize our record with respect to the newly resolved variations belonging to the modes of variability presented above. To achieve this, we analyze the characteristics of the individual events as well as the background climate in which they occur, inferred from complementary climate proxies (Fig. **??**). .

~~A feature common to TI and TII is~~

4.2 The 129-ka event

The 129-ka event refers to the pronounced increase in CH_4 and N_2O concentrations to interglacial levels at the end of ~~the respective deglaciation. The 128-ka event marking the onset of the Last Interglacial (LIG) appears as an analogue of the rise at the end of the Younger Dryas (YD), marking the onset of the Holocene.CH_4 and N_2O concentrations reached in the early interglacial times are approximately similar for the LIG and the Holocene (~720–740 ppb and ~270 ppb, respectively). The WD data show the onset of the CH_4 rise at the end of the YD to start from lower values (~480 ppb compared to ~530 ppb at ~128 ka BP) making this increase larger in magnitude by ~70 ppb. Moreover, the somewhat shorter timescale of this increase (less than 200 years compared to ~300 years at ~128 ka BP in our data) and the overshoot at the end of the event can, at least partly, be explained by the smaller extent of smoothing in the WD data compared to our records (Rhodes et al., 2015; Nehrbass-Ahles et al., 2020). For N_2O, the amplitude and duration of the two events are approximately similar, exhibiting a ~30 ppb rise (from ~240 to 270 ppb) in ~800–900 years~~TII (Fig. 2). For both gases, this event accounts for about half of the deglacial change in concentrations.

~~At the end of the YD and at ~128 ka BP,~~ CH_4 and N_2O concentrations ~~rise~~ rose in parallel with the main resumption of the AMOC, as indicated by the evolution of the isotopic ratio of neodymium 143 and 144 (ε_{Nd}) (Deaney et al., 2017; Böhm et al., 2015)~~, and the associated northward shift of the ICTZ indicated by the~~ . At the same time, the evolution of the isotopic composition of speleothem calcite ($\delta^{18}O(CaCO_3)$) indicates a northward shift of the ITCZ (Cheng et al., 2009, 2016) (Fig. ~~??), in a manner consistent with DO-like variability. The~~ 3). These are fingerprints of DO-type variability. Accordingly, the abrupt CH_4 rise likely reflects the response of terrestrial emissions ~~likely~~ from NH tropical wetlands. The ~~simultaneity of the N_2O increase~~ simultaneous increase in both gases indicates that terrestrial emissions contributed, at least partly, to the ~~128-ka event, similar to what has been demonstrated for TI on the basis of an isotopic deconvolution (Fischer et al., 2019) . The data of Deaney et al. (2017) suggest the main AMOC resumption to have~~ N_2O rise at ~129 ka BP. However, because the deglacial AMOC resumption occurred at this time~~. Therefore~~, it can be assumed that marine sources also played a role~~,~~ ~~consistent with what has been shown for the end of the YD (Schilt et al., 2014; Fischer et al., 2019)~~. A contribution from both marine and terrestrial emissions is in agreement with the findings of Schilt et al. (2014) and Fischer et al. (2019) for DO-type fluctuations during TI. Higher resolution measurements of the isotopic composition of N_2O combined with a deconvolution, similar to ~~Schilt et al. (2014) and Fischer et al. (2019)~~the aforementioned studies, are needed to quantitatively determine the relative contribution of the sources during the ~~128-ka~~ 129-ka event.

~~The 128-ka~~

4.3 The 130-ka event

The 129-ka event is preceded by a phase of rising N_2O concentrations in the interval from ~~130.5 to 129.8~~ 130.7 to 130 ka BP at the end of HS11 ~~(135–130 ka BP (Marino et al., 2015))~~ Fig. ~~??~~2). This is reminiscent of the pattern of late ~~stadial increases~~HS-type increase, where N_2O concentrations rose before ~~DO-like~~ the rapid DO-type Greenland temperature and CH_4

changes increases (Schilt et al., 2013). The timescale of the 130.5-ka 130-ka event is in the range of the duration typically observed for these episodes (∼0.5–2 millennia) (Schilt et al., 2013). On the other hand, , while the N_2O growth rate during our event appears slightly larger (∼3 ppb compared to typically ∼1 ppb per century).

The evolution of N_2O concentrations from 130.5 ka BP to the onset of the 128-ka event is remarkably coeval, within dating uncertainty, with the variability of $\delta^{18}O(CaCO_3)$ and of the isotopic composition of atmospheric oxygen ($\delta^{18}O(O_2)$) (Landais et al., 2013; Cheng et al., 2009) (Fig. **??**), also displaying an initial period of change followed by plateaus. At this timescale, $\delta^{18}O(CaCO_3)$ and $\delta^{18}O(O_2)$ reflect changes in the low latitude hydrological cycle driven by shifts in the ICTZ (Landais et al., 2010; Cheng et al., 2009). Taken at face value, they indicate a small intensification of the tropical hydroclimate at ∼130.5 ka BP prior to the DO-like fluctuation at ∼128 ka BP. This intensification has been interpreted as a transition from a HS to a DO stadial (Landais et al., 2013) and might be a consequence of the partial AMOC resumption reported in Böhm et al. (2015). In fact, the isotopic ratios of protactinium 231 and thorium 230 (^{231}Pa / ^{230}Th), reflecting the overturning rate of the AMOC, shows a decline to interglacial values substantially earlier than the decrease in ε_{Nd} occurring around ∼128 ka BP (Böhm et al., 2015) (Fig. **??**). The decoupling of the two oceanic tracers during part of TII has been interpreted as a change in the AMOC regime from the *off* mode, characteristic of HS (suppressed convection of northern-sourced water, extremely reduced overturning rates, high ε_{Nd}, and high ^{231}Pa / ^{230}Th) to the *cold* mode (shallow convection, vigorous overturning rate, high ε_{Nd}, and low ^{231}Pa / ^{230}Th) (Böhm et al., 2015), prevailing around glacial maxima. Additional evidence arguing for a partial resumption of the AMOC is given by the evolution of the isotopic composition of atmospheric nitrogen ($\delta^{15}N(N_2)$), a proxy for Antarctic temperature, displaying a marked leveling off at ∼130.5 ka BP, consistent with a SH temperature response to a slightly enhanced northern heat advection by the AMOC (Landais et al., 2013; WAIS Divide Project Members, 2015; EPICA Commun (Fig. **??**).

Taking the evidences together, we propose that the 130.5-ka event constitutes a response to the transition from a HS to a DO stadial, where the rise in concentrations is associated with the partial AMOC resumption. The lack of The lack of a concomitant CH_4 fluctuation suggests that only changes in marine sources contributed to the Nfluctuation suggests that only the marine source contributed to the N_2O increase. Overall, the 130.5-ka event fits into the framework of the late stadial events (Schilt et al., 2013, 2014; Fischer et al., 2019) and can be viewed as an analogue of the late O increase, in agreement with the findings of Schilt et al. (2014) and Fischer et al. (2019) for the late HS1 rise during TI. However, the rise. The change in marine emissions may be linked to a long-term adjustment of the nitrate and oxygen inventories in the upper-ocean after a period of AMOC interruption (Schmittner and Galbraith, 2008). Overall, despite the somewhat different rates of change, the 130-ka event likely constitutes an instance of a late-HS N_2O emission rate was slightly larger than evidenced for HS1 (as well as for similar events during the last glacial period)fluctuation during TII. The attribution of the 130.5-ka 130-ka feature to the pattern of late stadial increases HS increase would be strengthened by additional measurements of $\delta^{15}N(N_2O)$ and $\delta^{18}O(N_2O)$, allowing the unambiguous identification of the dominant source contributing to this event.

4.4 The 134-ka event

Turning to the 134-ka event, its occurrence within HS11 and the properties of the CH_4 increase (duration and amplitude) are reminiscent of the ~~intra-stadial~~ HS-type pattern of variability evidenced by Rhodes et al. (2015). ~~Intra-stadial~~ HS-type fluctuations resolved in the WD ice core fully developed within ~~~200–300~~ 90-190 years (Rhodes et al., 2015). The broader GAD of the EDC ice core ~~(~170 years for our record)~~ implies that any such ~~intra-stadial features have to~~ features would appear strongly dampened in our data. This is supported by continuous CH_4 measurements in the Vostok ice core, demonstrating the absence of the characteristic overshoot resolved in the WD ice core ~~for the~~ during HS4 ~~intra-stadial fluctuation~~ (Fourteau et al., 2020; Rhodes et al., 2015). Therefore, the sharpness and amplitude of the 134-ka event is not consistent with the picture of a substantially smoothed version of ~~an intra-stadial~~ a HS-type fluctuation. The ~70 ppb rise observed in the EDC record would translate into a WD signal exceeding by far the amplitude range ~~(~30–55 ppb)~~ of the HS1, HS2, HS4 and HS5 fluctuations (32–53 ppb) (Rhodes et al., 2015). Secondly, ~~intra-stadial~~ HS-type CH_4 variability is also characterized by abrupt CO_2 jumps, millennial-scale ~~increase~~ increases in $\delta^{18}O(O_2)$, enrichment in speleothem $\delta^{18}O(CaCO_3)$ and the absence of concomitant N_2O variability ~~(Bauska et al., 2016, 2018; Marcott et al., 2014; Fischer et al., 2019; Schilt et al., 2013, 2010a; Guillevic et al., 2014)~~(Bauska et al., 2016, . The simultaneous occurrence of the CH_4 and N_2O pulses at ~134 ka BP, the depletion in speleothem $\delta^{18}O(CaCO_3)$, and the lack of any fluctuation in the $\delta^{18}O(O_2)$ record (Landais et al., 2013) contradict these observations (Fig. ~~??~~ and ~~??~~3). The 134-ka event is therefore likely to have resulted from different mechanisms ~~than those driving intra-stadial variability and , consequently, cannot be considered as an analogue of the 16.15-ka event that developed within HS1 (Fig. ??).~~

and does not constitute an instance of a HS-type CH_4 fluctuation during TII. On the other hand, simultaneous rises of atmospheric CH_4 and N_2O concentrations are observed during ~~DO-like fluctuations. In~~ DO-type fluctuations. During the last glacial cycle, ~~interstadials typically lasted for~~ the amplitude of DO-type CH_4 increases ranges from ~~~1500 years with durations ranging from 240 to 14,380 years for Greenland Interstadial 3 and Greenland Interstadial 23, respectively (Rasmussen et al., 2014) . The onset of these interstadials were accompanied by increases in concentration ranging from~~ 50 to ~~260 ppb (CH_4) and from 10 to 40 ppb (N_2O) (Baumgartner et al., 2014; Schilt et al., 2013; Flückiger et al., 2004). The amplitude and duration of the CH_4 pulse at ~134 ka BP~~ 220 ppb in Greenland ice cores and elevated concentrations lasted for centuries to millennia (Baumgartner et al., 2014; Flückiger et al., 2004). Accordingly, the magnitude of the 134-ka event fits well within the amplitude range observed for the well resolved DO-type fluctuations in the EDC record of Loulergue et al. (2008) (~~~400 years, ~70 ppb)are well comparable to those observed for DO3, DO6, DO9, and DO10, where amplitudes are smaller or equal to 100 ppb (Baumgartner et al., 2014) and durations are shorter than 700 years (Rasmussen et al., 2014). For N_2O, the amplitude~~ 50-185 ppb). Going further, results from Greenland ice cores have shown that the amplitude of DO-type CH_4 rises tracks the variations in low to mid-latitude NH summer insolation, where the most substantial changes in concentration are associated with higher insolation. This indicates that the amount or seasonal distribution of solar radiation have modulated the response of CH_4 sources during interstadials (Brook et al., 1996; Flückiger et al., 2004). The 134-ka event occurs during a time period of low NH summer insolation (Fig. 2), comparable to this at DO2. Yet, the magnitude of the 134-ka event ~~compares well with those of DO-like fluctuations (Flückiger et al., 2004)~~appears larger (~70 ppb compared to ~50 ppb for DO2 in the EDC record).

Associating our event to a ~~DO-like~~ DO-type pattern of variability requires evidence for a northward shift of the ~~ICTZ~~ ITCZ and reinvigoration of the AMOC. Synchronous with the 134-ka event, within dating uncertainty, we observe a short-lived negative excursion in speleothem $\delta^{18}O(CaCO_3)$ records (Cheng et al., 2006) (Fig. ~~??~~3) as well as fluctuations in proxies reflecting salinity and runoff intensity in the Bay of Bengal (Nilsson-Kerr et al., 2019). These data indicate a transient strengthening of the NH tropical monsoon systems consistent with a northward shift of the ~~ICTZ~~ITCZ. Concerning the behavior of the AMOC, we are not aware of studies ~~elaborating on a possible~~ reporting on a potential reinvigoration at this time. Nevertheless, oceanic tracers exhibit a small and short-lived fluctuation in the time interval 133–132 ka BP (on the timescale of Böhm et al. (2015)) before reaching their maximum HS11 values (Böhm et al., 2015). On the updated chronology of the sediment core ODP Site 1063 (Deaney et al., 2017), the negative excursion in the ~~ϵ_{Nd}~~ε_{Nd}record of Böhm et al. (2015) coincides with a comparably small value in the data of Deaney et al. (2017) (Fig. ~~??~~2). However, the revised chronology places the excursion in ~~ϵ_{Nd}~~$\varepsilon_{Nd}$and ^{231}Pa / ^{230}Th substantially earlier ~~(onset~~ than the 134-ka event (Fig. 3). The onset of this excursion is at ~137.4 ka BP, corresponding to a shift by ~4.9 thousand of years with respect to the timescale of Böhm et al. (2015)~~) than the 134-ka event (Fig. ?? and ??).~~ . Since the timescale of the sediment core is tuned to the Antarctic Ice Core Chronology (AICC2012) (Bazin et al., 2013; Veres et al., 2013) within an estimated uncertainty of 400 years, the fluctuations resolved in the ice and marine cores ~~shall~~should, in principle, not be considered as synchronous. However, the alignment with the AICC2012 is performed using only one tie point between CH_4 and the isotopic composition of planktonic foraminifera (at ~128.7 ka BP, corresponding to the abrupt CH_4 increase into the LIG) (Deaney et al., 2017). Therefore, ~~we keep the possibility open~~ it may be possible that the two timescales are less tightly aligned away from ~~the tie point suggest that an occurrence of~~ this tie point. If this would be the case, it could be hypothesized that the excursions in oceanic proxies are synchronous with the fluctuations of $\delta^{18}O(CaCO_3$ ~~and trace gases might still be possible. DO-like~~ , CH_4 and N_2O.

DO-type variability is typically also imprinted in the ~~$\delta^{15}N(N_2)$~~ temperature record from Antarctic ice cores as well as in the $\delta^{18}O(O_2)$ record. However, ~~changes in~~ the responses of these proxies are generally ~~subtle~~ attenuated or occurring on longer timescales compared to those of CH_4 and $\delta^{18}O(CaCO_3)$~~, especially for $\delta^{18}O(O_2)$ (Landais et al., 2010)~~. Accordingly, ~~the duration or amplitude of the 134-ka event~~ a short and small-amplitude interstadial at ~134 ka BP might not have ~~been sufficient to produce a discernible signal in the~~ left discernible imprints in the respective records of Landais et al. (2013) and Jouzel et al. (2007) (Fig. ~~??~~). 2 and 3).

Taking the proxy evidences together, we speculate that a brief and small-scale resumption of the AMOC might have occurred within HS11, accounting for the northward ICTZ shift and the rise in atmospheric CH_4 and N_2O concentrations~~, consistent with the picture of DO-like variability~~. We acknowledge that our interpretation is limited by the relatively coarse resolution of ~~ϵ_{Nd}~~$\varepsilon_{Nd}$and ^{231}Pa / ^{230}Th as well as by the uncertainty arising from cross-dating sediment and ice core records. ~~It should finally be noted that the simultaneity of the CH_4 and~~ Concerning N_2O~~increase and~~ , we finally note that the duration of the ~~rising phase is consistent only with a contribution from~~ rise and the simultaneity with the excursion in CH_4 suggest that terrestrial N_2O ~~sources~~ emissions contributed by far the most to the 134-ka event (Fischer et al., 2019).

Should our interpretation hold, the 134-ka event can be considered as a short ~~DO-event, contrasting with the marked Bølling–Allerød (BA) fluctuationduring TI (Fig. ??). This raises the question of why the oceanic circulation was unable to~~

recover in the same way as during the BA. Because the 134-ka event coincides, within dating uncertainty, with the occurrence of DO-type fluctuation. We speculate that the hypothesized AMOC reinvigoration might have been perturbed by Meltwater Pulse 2B (MWP–2B)(Fig. **??**), it would be tempting to link the quenching of the emerging interstadial at ~134 ka BP to freshwater forcing. MWP-2B). MWP-2B constitutes the major melting event in the course of TII. As a matter of fact, it contributed represents ~70 m of sea-level rise (~70 % of the deglacial change) and mainly entered into the North-Atlantic along with substantial volumes of icebergs, as indicated by the elevated occurrence of ice rafted debris recorded in sediment cores at this time (Marino et al., 2015; Grant et al., 2014; Skinner and Shackleton, 2006) sea-level change and coincides with the 134-ka event within dating uncertainty (Fig. **??**) .

However, the concept of freshwater forcing as a trigger of AMOC shutdown (either as iceberg discharges during HS or MWPs during glacial terminations) has become a matter of intense debate. Firstly, the history of MWPs is decoupled from that of the AMOC and Greenland temperature in the course of TI (most notably exemplified by the absence of any such pulses for the YD stadial) (Tarasov and Peltier, 2005; Stanford et al., 2006). Secondly, iceberg discharge events within HS are consistently lagging behind oceanic circulation and Greenland temperature changes (Barker et al., 2015; Henry et al., 2016) . The current paradigm rather considers freshwater forcing as resulting from AMOC declines. This view is supported by modeling and experimental studies demonstrating that the interior of the ocean accumulates heat at times the AMOC collapses (Galbraith et al., 2016; Pedro et al., 2018; Bereiter et al., 2018; Baggenstos et al., 2019), constituting a potent forcing for destabilizing glacial ice sheets and producing bursts of meltwater (Flückiger et al., 2006; Marcott et al., 2011; Clark et al., 2020; Galbraith et al., 2016) . In summary, we are currently unable to propose a mechanism accounting for the relative brevity of the 134-ka event.

Summarizing the evidences, we note that the outstanding fluctuations in CH_4 and N_2O concentrations during 2) (Marino et al., 2015) . The disruption of the penultimate deglaciation are all instances of recurrent modes of variability, also evidenced during the last deglaciation as well as during oceanic circulation by freshwater forcing might have been enabled by the high susceptibility of the AMOC to perturbations at a time when the high-latitude SH was particularly cold (Buizert and Schmittner, 2015), as was the case during HS11 (Fig. 2). This situation favors the occurence of relatively short, centennial, interstadials such as those appearing near the last glacial periodmaximum in Greenland ice cores.

5 Conclusions

In the present study, we increased the resolution of the deglacial CH_4 and N_2O records, allowing us to derive composite datasets covering TII (140–128 ka BP) at average resolutions of ~100 years. Our results display pronunced fluctuations standing out of the overall transition of CH_4 and N_2O concentrations to interglacial conditions. The most prominent one is resolved placed at ~128 129 ka BP and constitutes an analogue of the rise at the end of the YD during the last terminationdelineates the transition into the LIG. We assume that terrestrial and marine sources contributed to the N_2O increase at this time. Additionally, we now entirely identify the unequivocally identify a 134 and 130.5-ka 130-ka event. We link the latter to the pattern of late stadial HS-type N_2O increase, where changes in marine emissions are likely to be the only contributor. The former is regarded as a short DO-like DO-type fluctuation, whose timescale indicates that only terrestrial N_2O sources likely contributed to the

increase. We note that these fluctuations in CH_4 and N_2O concentrations during the penultimate deglaciation are all instances of recurrent modes of variability, also evidenced during the last deglaciation as well as during the last glacial period.

Data availability. Data will be made available online on the NOAA paleoclimate database.

Appendix A: New measurement system for CH_4 and N_2O

Although gas chromatography (GC) have been used extensively to measure CH_4 and N_2O at the University of Bern (e.g. Flückiger et al., 1999, 2002, 2004; Baumgartner et al., 2012, 2014; Loulergue et al., 2008; Schilt et al., 2010a, b, 2013; Spahni et al., , the totally revised extraction and GC setup presented here has not been described before. The device is composed of different functional units, enabling the different actions of the system (standard injection, extraction, separation and detection) (colored boxes in Fig. 4). The measurements are carried out using three distinct lines. The ice line (IL, under vacuum, red path in Fig. 4) is used to extract air from ice core samples. The continuous-flow line (CFL, flushed with He, green path in Fig. 4) is used to measure standards to calibrate ice core measurements. Standards and samples are introduced differently into the separation unit to gain time during daily operation. Therefore, following the identical treatment principle, we also employ the standard over ice line (SOIL, blue line in Fig. 4) to periodically inject standards for comparison with similar measurements performed with the CFL in order to account for contamination stemming from the IL. The mean offset between the lines is used to correct IL data.

To extract gas from ice core samples, we use continuous extraction under vacuum. Air is released from the ice during the melting (immersing the bottom of the vessel in a $\sim$20°C water bath) and is simultaneously adsorbed on an activated charcoal trap held at -196°C using liquid nitrogen (T2 in Fig. 4). Water vapor is condensed beforehand using another cold trap held at -80°C (T1 in Fig. 4). The progression of the extraction is monitored with a pressure gauge (P5 in Fig. 4). The completion of the extraction is indicated by a P5 pressure value $\leqslant$ 0.25 mbar. When this value is reached, T2 is isolated from the vessel and heated to facilitate CH_4 and N_2O desorption from the charcoal bed. The duration and final temperature of the heating (5 min, 130°C) ensure full recovery of the adsorbed gas. At the end of this phase, He flushes the content of T2 into the separation unit. Overall, the advantage of our procedure is the permanently low CH_4 and N_2O partial pressure, as well as total air pressure, prevailing in the vessel during the extraction. Accordingly, equilibrium conditions with respect to solubility are never reached, precluding the need of a solubility correction. This type of correction was required in traditional analyses using a melt-refreeze method, where the air sample is enclosed in the vessel head space during the extraction.

CH_4 and N_2O are separated from the bulk air in the separation unit before reaching the detection unit equipped with a thermal conductivity detector (TCD), a flame-ionization detector (FID) and an electron-capture detector (ECD) to quantify the amount of air, CH_4 and N_2O, respectively. The separation unit is composed of a succession of GC columns. CH_4 and N_2O are separated from the bulk air in the precolumn and analytical column (Fig. 4). After detection of the air peak by the TCD, V8 allows to route CH_4 towards the FID (via T5 and T7) and N_2O towards the ECD (via T4 and T6) (Fig. 4). T5 and T4 are used to separate CH_4 and N_2O, respectively, from species having almost similar retention times. T7 and T6 are used to focus the gas to obtain sharp peaks in the chromatograph.

The amount of air, CH_4 and N_2O is quantified by integrating the area below the corresponding GC peaks. For each species, calibration curves are established between areas and the number of moles calculated using the volume, temperature and pressure of the sample loop as well as the known CH_4 and N_2O mole fractions of the standard gases. We use a set of primary standards provided by the National Oceanic and Atmospheric Administration and referenced to the World Meteorological Organisation mole fraction scales: WMOX2004A scale (CH_4) and NOAA-2006A (N_2O) (Dlugokencky et al., 2005; Hall et al., 2007). This set of standards brackets the glacial-interglacial range of CH_4 (358.88±0.16 ppb, 838.59±0.28 ppb, and 1729.30±0.34 ppb) and N_2O concentrations (187.10±0.12 ppb, 194.13±0.12 ppb, and 300.20±0.12 ppb). CH_4 and N_2O mole fractions are calculated by dividing the number of CH_4 and N_2O moles by the number moles of air. In addition, Total Air Content can also be quantified using the TCD area as well as the volume, temperature and pressure of the sample loop.

After calibration, the results are corrected for the line offset between CFL and SOIL. This offset accounts for the blank introduced in the IL and is averaged over, at least, a measurement campaign. The CH_4 and N_2O line offsets appear to be linearly dependent on the concentration enabling the use of linear interpolations to correct ice core results.

The uncertainty of the CH_4 and N_2O data derived with our instrument amounts to 7 ppb and 6 ppb, respectively. It is calculated as sum of the individual uncertainty, associated with the overall analytical procedure (1σ standard deviation of SOIL measurements) and with the line offset correction, in quadrature.

Appendix B: Construction of composite CH_4 and N_2O records

The construction of the composite records presented in this study is complicated by offsets between the datasets, where our results appear on average 18±10 ppb (CH_4) and 21±3 ppb (N_2O) higher than previous data, although all datasets show the same relative changes (Fig. 5). The offsets are calculated as the mean of the residuals between splines with cut-off periods of 10 thousand years fitted through the datasets. We computed splines according to Enting (1987), using the same routine as Beck et al. (2018), where each spline is the average of 1000 iterations with data points varied within a normal distribution inside their uncertainty range.

It seems likely that the offsets are linked to the different extraction techniques employed. In fact, the published EDC data were measured at the University of Bern and Grenoble with instruments using melt-refreeze extraction (Loulergue et al., 2008; Schilt et al., 2010a). Melt-refreeze extraction is prone to underestimate CH_4 and N_2O concentrations if the refreezing is not perfectly efficient, while in our method air is quantitatively extracted from the ice samples. We note that also the values presented in previous publications had to be aligned for interlaboratory offsets on the order of 10 ppb for CH_4 (Loulergue et al., 2008), which may also reflect differences in the extraction efficiency of previously used melt-refreeze methods in different labs. Because melt-refreeze extraction has been the standard procedure for decades and the EDC records have been measured exclusively using this technique. We therefore think that additional overlapping measurements with an independent extraction technique (e.g. sublimation) are needed to resolve the dispute. Without further evidence, we prefer striving for consistency by correcting our data to the EDC benchmark records of Loulergue et al. (2008) and Schilt et al. (2010a). To achieve this, we subtract the mean offsets of 18 ppb (CH_4) and 21 ppb (N_2O) from our results. This approach is facilitated by the high degree of co-variation between the datasets (Fig. 5).

The merging procedure described above adds an additional source of uncertainty to our results. Accounting for the uncertainty of the mean offset, taken as the standard deviation (1σ) of the residuals between the splines, increases the total uncertainty of the new data included in the composite records to 12 ppb (CH_4) and 8 ppb (N_2O). For the published EDC values and the isotopic measurements, the uncertainties amount to 10 ppb (CH_4), 4 ppb (N_2O), 0.22 ‰ ($\delta^{15}N(N_2O)$), and 0.34 ‰ ($\delta^{18}O(N_2O)$), as reported in Loulergue et al. (2008), Schilt et al. (2010a) and Schmitt et al. (2014).

Author contributions. The present study was designed by T.F.S, H.F and L.S. L.S and J.H performed the methane and nitrous oxide measurements. J.S provided the isotopic data. L.S wrote the text with inputs from all authors.

Competing interests. The authors declare that they have no conflict of interest.

Acknowledgements. The authors would like to thank Barbara Seth for the measurements of the isotopic composition of N_2O, Gregory Teste for assistance in cutting ice samples, as well as Michael Bock and Jan Strähl for the construction of the new CH_4 and N_2O measurement system. We acknowledge financial support by the Swiss National Science Foundation (SNF project numbers 200020_172745and , 200020_200492,200020_172506 and 200020_200511). This work is a contribution to the *European Project for Ice Coring in Antarctica* (EPICA), a joint European Science Foundation/European Commission scientific program, funded by the European Union and by national contributions from Belgium, Denmark, France, Germany, Italy, The Netherlands, Norway, Sweden, Switzerland, and the United Kingdom. The main logistic support was provided by IPEV and PNRA. This is EPICA publication no. XX.

References

Alley, R. B.: Wally was right: Predictive ability of the North Atlantic "conveyor belt" hypothesis for abrupt climate change, Annu. Rev. Earth Pl. Sc., 35, 241–272, https://doi.org/10.1146/annurev.earth.35.081006.131524, 2007.

Baggenstos, D., Häberli, M., Schmitt, J., Shackleton, S. A., Birner, B., Severinghaus, J. P., Kellerhals, T., and Fischer, H.: Earth's radiative imbalance from the Last Glacial Maximum to the present, P. Natl. Acad. Sci. USA, 116, 14 881–14 886, https://doi.org/10.1073/pnas.1905447116, 2019.

Barker, S., Chen, J., Gong, X., Jonkers, L., Knorr, G., and Thornalley, D.: Icebergs not the trigger for North Atlantic cold events, Nature, 520, 333–336, https://doi.org/10.1038/nature14330, 2015.

Baumgartner, M., Schilt, A., Eicher, O., Schmitt, J., Schwander, J., Spahni, R., Fischer, H., and Stocker, T. F.: High–resolution interpolar difference of atmospheric methane around the Last Glacial Maximum, Biogeosciences, 9, 3961–3977, https://doi.org/10.5194/bg-9-3961-2012, 2012.

Baumgartner, M., Kindler, P., Eicher, O., Floch, G., Schilt, A., Schwander, J., Spahni, R., Capron, E., Chappellaz, J., Leuenberger, M., Fischer, H., and Stocker, T. F.: NGRIP CH_4 concentration from 120 to 10 kyr before present and its relation to a $\delta^{15}N$ temperature reconstruction from the same ice core, Clim. Past, 10, 903–920, https://doi.org/10.5194/cp-10-903-2014, 2014.

Bauska, T. K., Baggenstos, D., Brook, E. J., Mix, A. C., Marcott, S. A., Petrenko, V. V., Schaefer, H., Severinghaus, J. P., and Lee, J. E.: Carbon isotopes characterize rapid changes in atmospheric carbon dioxide during the last deglaciation, P. Natl. Acad. Sci. USA, 113, 3465–3470, https://doi.org/10.1073/pnas.1513868113, 2016.

Bauska, T. K., Brook, E. J., Marcott, S. A., Baggenstos, D., Shackleton, S., Severinghaus, J. P., and Petrenko, V. V.: Controls on millennial–scale atmospheric CO_2 variability during the last glacial period, Geophys. Res. Lett., 45, 7731–7740, https://doi.org/10.1029/2018GL077881, 2018.

Bauska, T. K., Marcott, S. A., and Brook, E. J.: Abrupt changes in the global carbon cycle during the last glacial period, Nature Geoscience, 14, 91–96, 2021.

Bazin, L., Landais, A., Lemieux-Dudon, B., Kele, H. T. M., Veres, D., Parrenin, F., Martinerie, P., Ritz, C., Capron, E., and Lipenkov, V. Y.: An optimized multi–proxy, multi-site Antarctic ice and gas orbital chronology (AICC2012): 120–800 ka, Clim. Past, 9, 1715–1731, https://doi.org/10.5194/cp-9-1715-2013, 2013.

Beck, J., Bock, M., Schmitt, J., Seth, B., Blunier, T., and Fischer, H.: Bipolar carbon and hydrogen isotope constraints on the Holocene methane budget, Biogeosciences, 15, 7155–7175, https://doi.org/10.5194/bg-15-7155-2018, 2018.

Bereiter, B., Shackleton, S. A., Baggenstos, D., Kawamura, K., and Severinghaus, J. P.: Mean global ocean temperatures during the last glacial transition, Nature, 553, 39–44, https://doi.org/10.1038/nature25152, 2018.

Berger, A. and Loutre, M.-F.: Insolation values for the climate of the last 10 million years, Quaternary Science Reviews, 10, 297–317, 1991.

Bloom, A. A., Palmer, I. P., Fraser, A., Reay, D. S., and Frankenberg, C.: Large–scale controls of methanogenesis inferred from methane and gravity spaceborne data, Science, 327, 322–325, https://doi.org/10.1126/science.1175176, 2010.

Bock, M., Schmitt, J., Möller, L., Spahni, R., Blunier, T., and Fischer, H.: Hydrogen isotopes preclude marine hydrate CH_4 emissions at the onset of Dansgaard–Oeschger events, Science, 328, 1686–1689, https://doi.org/10.1126/science.1187651, 2010.

Bock, M., Schmitt, J., Beck, J., Seth, B., Chappellaz, J., and Fischer, H.: Glacial/interglacial wetland, biomass burning, and geologic methane emissions constrained by dual stable isotopic CH_4 ice core records, P. Natl. Acad. Sci. USA, 114, E5778–E5786, https://doi.org/10.1073/pnas.1613883114, 2017.

Böhm, E., Lippold, J., Gutjahr, M., Frank, M., Blaser, P., Antz, B., Fohlmeister, J., Frank, N., Andersen, M. B., and Deininger, M.: Strong and deep Atlantic meridional overturning circulation during the last glacial cycle, Nature, 517, 73–76, https://doi.org/10.1038/nature14059, 2015.

Broccoli, A. J., Dahl, K. A., and Stouffer, R. J.: Response of the ICTZ to Northern Hemisphere cooling, Geophys. Res. Lett., 33, https://doi.org/10.1029/2005GL024546, 2006.

Brook, E. J., Sowers, T., and Orchardo, J.: Rapid variations in atmospheric methane concentration during the past 110,000 years, Science, 273, 1087–1091, 1996.

Buizert, C. and Schmittner, A.: Southern Ocean control of glacial AMOC stability and Dansgaard-Oeschger interstadial duration, Paleoceanography, 30, 1595–1612, 2015.

Buizert, C., Sigl, M., Severi, M., Markle, B. R., Wettstein, J. J., McConnell, J. R., Pedro, J. B., Sodemann, H., Goto-Azuma, K., Kawamura, K., Fujita, S., Motoyama, H., Hirabayashi, M., Uemura, R., Stenni, B., Parrenin, F., He, F., Fudge, T. J., and Steig, E. J.: Abrupt ice–age shifts in southern westerly winds and Antarctic climate forced from the north, Nature, 563, 681–685, https://doi.org/10.1038/s41586-018-0727-5, 2018.

Cheng, H., Edwards, R. L., Wang, Y., Kong, X., Ming, Y., Kelly, M. J., Wang, X., Gallup, C. D., and Liu, W.: A penultimate glacial monsoon record from Hulu Cave and two-phase glacial terminations, Geology, 34, 217–220, https://doi.org/10.1130/G22289.1, 2006.

Cheng, H., Edwards, R. L., Broecker, W. S., Denton, G. H., Kong, X., Wang, Y., Zhang, R., and Wang, X.: Ice age terminations, Science, 326, 248–252, https://doi.org/10.1126/science.1177840, 2009.

Cheng, H., Edwards, R. L., Sinha, A., Spötl, C., Yi, L., Chen, S., Kelly, M., Kathayat, G., Wang, X., Li, X., Kong, X., Wang, Y., Ning, Y., and Zhang, H.: The Asian monsoon over the past 640,000 years and ice age terminations, Nature, 534, 640–646, https://doi.org/10.1038/nature18591, 2016.

Clark, P. U., He, F., Golledge, N. R., Mitrovica, J. X., Dutton, A., Hoffman, J. S., and Dendy, S.: Oceanic forcing of penultimate deglacial and last interglacial sea–level rise, Nature, 577, 660–664, https://doi.org/10.1038/s41586-020-1931-7, 2020.

Deaney, E. L., Barker, S., and Van de Flierdt, T.: Timing and nature of AMOC recovery across Termination II and magnitude of deglacial CO_2 change, Nat. Commun., 8, 1–10, https://doi.org/10.1038/ncomms14595, 2017.

Dlugokencky, E. J., Myers, R. C., Lang, P. M., Masarie, K. A., Crotwell, A. M., Thoning, K. W., Hall, B. D., Elkins, J. W., and Steele, L. P.: Conversion of NOAA atmospheric dry air CH_4 mole fractions to a gravimetrically prepared standard scale, J. Geophys. Res.-Atmos., 110, https://doi.org/10.1029/2005JD006035, 2005.

Dyonisius, M. N., Petrenko, V. V., Smith, A. M., Hua, Q., Yang, B., Schmitt, J., Beck, J., Seth, B., Bock, M., Hmiel, B., Vimont, I., Menking, J. A., Shackleton, S. A., Baggenstos, D., Bauska, T. K., Rhodes, R. H., Sperlich, P., Beaudette, R., Harth, C., Kalk, M., Brook, E. J., Fischer, H., Severinghaus, J. P., and Weiss, R. F.: Old carbon reservoirs were not important in the deglacial methane budget, Science, 367, 907–910, https://doi.org/10.1126/science.aax0504, 2020.

Enting, I.: On the use of smoothing splines to filter CO_2 data, J. Geophys. Res.-Atmos., 92, 10 977–10 984, https://doi.org/10.1029/JD092iD09p10977, 1987.

EPICA Community Members: One–to–one coupling of glacial climate variability in Greenland and Antarctica., Nature, 444, 195, https://doi.org/10.1038/nature05301, 2006.

Epifanio, J. A., Brook, E. J., Buizert, C., Edwards, J. S., Sowers, T. A., Kahle, E. C., Severinghaus, J. P., Steig, E. J., Winski, D. A., Osterberg, E. C., Fudge, T. J., Aydin, M., Hood, E., Kalk, M., Kreutz, K. J., Ferris, D. G., and Kennedy, J. A.: The SP19 chronology for the South Pole Ice Core–Part 2: gas chronology, Δage, and smoothing of atmospheric records, Climate of the Past, 16, 2431–2444, 2020.

Fischer, H., Meissner, K. J., Mix, A. C., Abram, N. J., Austermann, J., Brovkin, V., Capron, E., Colombaroli, D., Daniau, A.-L., Dyez, K. A., Felis, T., Finkelstein, S. A., Jaccard, S. L., McClymont, E. L., Rovere, A., Sutter, J., Wolff, E. W., Affolter, S., Bakker, P., Ballesteros-Ctánovas, J. A., Barbante, C., Caley, T., Carlson, A. E., Churakova (Sidorova), O., Cortese, G., Cumming, B. F., Davis, B. A. S., de Vernal, A., Emile-Geay, J., Fritz, S. C., Gierz, P., Gottschalk, J., Holloway, M. D., Joos, F., Kucera, M., Loutre, M.-F., Lunt, D. J., Marcisz, K., Marlon, J. R., Martinez, P., Masson-Delmotte, V., Nehrbass-Ahles, C., Otto-Bliesner, B. L., Raible, C. C., Risebrobakken, B., Sánchez Goñi, M. F., Saleem Arrigo, J., Sarnthein, M., Sjolte, J., Stocker, T. F., Velasquez Alvárez, P. A., Tinner, W., Valdes, P. J., Vogel, H., Wanner, H., Yan, Q., Yu, Z., Ziegler, M., and Zhou, L.: Palaeoclimate constraints on the impact of 2°C anthropogenic warming and beyond, Nat. Geosci., 11, 474, https://doi.org/10.1038/s41561-018-0146-0, 2018.

Fischer, H., Schmitt, J., Bock, M., Seth, B., Joos, F., Spahni, R., Lienert, S., Battaglia, G., Stocker, B. D., Schilt, A., and Brook, E. J.: N_2O changes from the Last Glacial Maximum to the preindustrial–Part 1: Quantitative reconstruction of terrestrial and marine emissions using N_2O stable isotopes in ice cores, Biogeosciences, 16, 3997–4021, https://doi.org/10.5194/bg-16-3997-2019, 2019.

Flückiger, J., Dällenbach, A., Blunier, T., Stauffer, B., Stocker, T. F., Raynaud, D., and Barnola, J.-M.: Variations in atmospheric N_2O concentration during abrupt climatic changes, Science, 285, 227–230, https://doi.org/10.1126/science.285.5425.227, 1999.

Flückiger, J., Monnin, E., Stauffer, B., Schwander, J., Stocker, T. F., Chappellaz, J., Raynaud, D., and Barnola, J.-M.: High–resolution Holocene N_2O ice core record and its relationship with CH_4 and CO_2, Global Biogeochem. Cy., 16, 10–1, https://doi.org/10.1029/2001GB001417, 2002.

Flückiger, J., Blunier, T., Stauffer, B., Chappellaz, J., Spahni, R., Kawamura, K., Schwander, J., Stocker, T. F., and Dahl-Jensen, D.: N_2O and CH_4 variations during the last glacial epoch: Insight into global processes, Global Biogeochem. Cy., 18, https://doi.org/10.1029/2003GB002122, 2004.

Flückiger, J., Knutti, R., and White, J. W. C.: Oceanic processes as potential trigger and amplifying mechanisms for Heinrich events, Paleoceanography, 21, https://doi.org/10.1029/2005PA001204, 2006.

Fourteau, K., Faïn, X., Martinerie, P., Landais, A., Ekaykin, A. A., Lipenkov, V. Y., and Chappellaz, J.: Analytical constraints on layered gas trapping and smoothing of atmospheric variability in ice under low-accumulation conditions, Clim. Past, 13, 1815, https://doi.org/10.5194/cp-13-1815-2017, 2017.

Fourteau, K., Martinerie, P., Faïn, X., Ekaykin, A. A., Chappellaz, J., and Lipenkov, V. Y.: Estimation of gas record alteration in very low accumulation ice cores, Clim. Past, 16, 503–522, https://doi.org/10.5194/cp-16-503-2020, 2020.

Galbraith, E. D., Merlis, T. M., and Palter, J. B.: Destabilization of glacial climate by the radiative impact of Atlantic Meridional Overturning Circulation disruptions, Geophys. Res. Lett., 43, 8214–8221, https://doi.org/10.1002/2016GL069846, 2016.

Grant, K. M., Rohling, E. J., Ramsey, B. C., Cheng, H., Edwards, R. L., Florindo, F., Heslop, D., Marra, F., Roberts, A. P., Tamisiea, M. E., and Williams, F.: Sea–level variability over five glacial cycles, Nat. Commun., 5, 1–9, https://doi.org/10.1038/ncomms6076, 2014.

Guillevic, M., Bazin, L., Landais, A., Stowasser, C., Masson-Delmotte, V., Blunier, T., Eynaud, F., Falourd, S., Michel, E., Minster, B., Popp, T., Prié, F., and Vinther, B. M.: Evidence for a three–phase sequence during Heinrich Stadial 4 using a multiproxy approach based on Greenland ice core records, Climate of the Past, 10, 2115–2133, https://doi.org/10.5194/cp-10-2115-2014, 2014.

Hall, B. D., Dutton, G. S., and Elkins, J. W.: The NOAA nitrous oxide standard scale for atmospheric observations, J. Geophys. Res.-Atmos., 112, https://doi.org/10.1029/2006JD007954, 2007.

Hemming, S. R.: Heinrich events: Massive late Pleistocene detritus layers of the North Atlantic and their global climate imprint, Rev. Geophys., 42, https://doi.org/10.1029/2003RG000128, 2004.

Henry, L. G., McManus, J. F., Curry, W. B., Roberts, N. L., Piotrowski, A. M., and Keigwin, L. D.: North Atlantic ocean circulation and abrupt climate change during the last glaciation, Science, 353, 470–474, https://doi.org/10.1126/science.aaf5529, 2016.

Hopcroft, P. O., Valdes, P. J., O'Connor, F. M., Kaplan, J. O., and Beerling, D. J.: Understanding the glacial methane cycle, Nat. Commun., 8, 1–10, https://doi.org/10.1038/ncomms14383, 2017.

Huber, C., Leuenberger, M., Spahni, R., Flückiger, J., Schwander, J., Stocker, T. F., Johnsen, S., Landais, A., and Jouzel, J.: Isotope calibrated Greenland temperature record over Marine Isotope Stage 3 and its relation to CH_4, Earth. Planet. Sc. Lett., 243, 504–519, https://doi.org/10.1016/j.epsl.2006.01.002, 2006.

Joos, F., Battaglia, G., Fischer, H., Jeltsch-Thömmes, A., and Schmitt, J.: Marine N_2O emissions during a Younger Dryas-like event: the role of meridional overturning, tropical thermocline ventilation, and biological productivity, Environ. Res. Lett., 14, 075 007, https://doi.org/10.1088/1748-9326/ab2353, 2019.

Joos, F., Spahni, R., Stocker, B. D., Lienert, S., Müller, J., Fischer, H., Schmitt, J., Prentice, C. I., Otto-Bliesner, B., and Liu, Z.: N_2O changes from the Last Glacial Maximum to the preindustrial–Part 2: terrestrial N_2O emissions and carbon–nitrogen cycle interactions, Biogeosciences, 17, 3511–3543, https://doi.org/10.5194/bg-2019-118, 2020.

Jouzel, J., Masson-Delmotte, V., Cattani, O., Dreyfus, G., Falourd, S., Hoffmann, G., Minster, B., Nouet, J., Barnola, J.-M., Chappellaz, J., et al.: Orbital and millennial Antarctic climate variability over the past 800,000 years, science, 317, 793–796, 2007.

Landais, A., Dreyfus, G., Capron, E., Masson-Delmotte, V., Sanchez-Goni, M. F., Desprat, S., Hoffmann, G., Jouzel, J., Leuenberger, M., and Johnsen, S.: What drives the millennial and orbital variations of $\delta^{18}O_{atm}$?, Quaternary. Sci. Rev., 29, 235–246, https://doi.org/10.1038/ngeo1985, 2010.

Landais, A., Dreyfus, G., Capron, E., Jouzel, J., Masson-Delmotte, V., Roche, D. M., Prié, F., Caillon, N., Chappellaz, J., Leuenberger, M., Lourantou, A., Parrenin, F., Raynaud, D., and Teste, G.: Two-phase change in CO_2, Antarctic temperature and global climate during Termination II, Nat. Geosci., 6, 1062–1065, https://doi.org/10.1038/ngeo1985, 2013.

Levine, J. G., Wolff, E. W., Hopcroft, P. O., and Valdes, P. J.: Controls on the tropospheric oxidizing capacity during an idealized Dansgaard–Oeschger event, and their implications for the rapid rises in atmospheric methane during the last glacial period, Geophys. Res. Lett., 39, https://doi.org/10.1029/2012GL051866, 2012.

Loulergue, L., Schilt, A., Spahni, R., Masson-Delmotte, V., Blunier, T., Lemieux-Dudon, B., Barnola, J.-M., Raynaud, D., Stocker, T. F., and Chappellaz, J.: Orbital and millennial-scale features of atmospheric CH_4 over the past 800,000 years, Nature, 453, 383–386, https://doi.org/10.1038/nature06950, 2008.

Marcott, S. A., Clark, P. U., Padman, L., Klinkhammer, G. P., Springer, S. R., Liu, Z., Otto-Bliesner, B., Carlson, A. E., Ungerer, A., Padman, J., Feng, H., Cheng, J., and Schmittner, A.: Ice–shelf collapse from subsurface warming as a trigger for Heinrich events, P. Natl. Acad. Sci. USA, 108, 13 415–13 419, https://doi.org/10.1073/pnas.1104772108, 2011.

Marcott, S. A., Bauska, T. K., Buizert, C., Steig, E. J., Rosen, J. L., Cuffey, K. M., Fudge, T. J., Severinghaus, J. P., Ahn, J., Kalk, M. L., McConnell, J. R., Sowers, T., Taylor, K. C., White, J. W. C., and Brook, E. J.: Centennial–scale changes in the global carbon cycle during the last deglaciation, Nature, 514, 616–619, https://doi.org/10.1038/nature13799, 2014.

Marino, G., Rohling, E. J., Rodríguez-Sanz, L., Grant, K. M., Heslop, D., Roberts, A. P., Stanford, J. D., and Yu, J.: Bipolar seesaw control on last interglacial sea level, Nature, 522, 197–201, https://doi.org/10.1038/nature14499, 2015.

Melton, J., Wania, R., Hodson, E. l., Poulter, B., Ringeval, B., Spahni, R., Bohn, T., Avis, C., Beerling, D., Chen, G., Eliseev, A., Denisov, S., Hopcroft, P., Lettenmaier, D., Riley, W. J., Singarayer, J. S., Subin, Z. M., Tian, H., Zürcher, S., Brovkin, V., van Bodegom, P. M.,

Kleinen, T., Yu, Z. C., and Kaplan, J. O.: Present state of global wetland extent and wetland methane modelling: conclusions from a model inter–comparison project (WETCHIMP), Biogeosciences, 10, 753–788, https://doi.org/10.5194/bg-10-753-2013, 2013.

Myhre, G., Shindell, D., Bréon, F. M., Collins, W., Fuglestvedt, J., Huang, J., Koch, D., Lamarque, J. F., Lee, D., Mendoza, B., Nakajima, T., Robock, A., Stephens, G., T, T., and Zhang, H.: Anthropogenic and Natural Radiative Forcing, in: Climate Change 2013: The Physical Science Basis. Contribution of Working Group I to the Fifth Assessment Report of the Intergovernmental Panel on Climate Change, pp. 659–740, Cambridge: Cambridge University Press, https://doi.org/10.1017/CBO9781107415324.018, 2013.

Nehrbass-Ahles, C., Shin, J., Schmitt, J., Bereiter, B., Joos, F., Schilt, A., Schmidely, L., Silva, L., Teste, G., Grilli, R., Chappellaz, J., Hodell, D., Fischer, H., and Stocker, T. F.: Abrupt CO_2 release to the atmosphere under glacial and early interglacial climate conditions, Science, 369, 1000–1005, https://doi.org/10.1126/science.aay8178, 2020.

Nilsson-Kerr, K., Anand, P., Sexton, P. F., Leng, M. J., Misra, S., Clemens, S. C., and Hammond, S. J.: Role of Asian summer monsoon subsystems in the inter-hemispheric progression of deglaciation, Nat. Geosci., 12, 290–295, https://doi.org/10.1038/s41561-019-0319-5, 2019.

Oyabu, I., Kawamura, K., Kitamura, K., Dallmayr, R., Kitamura, A., Sawada, C., Severinghaus, J. P., Beaudette, R., Orsi, A., Sugawara, S., Ishidoya, S., Goto-Azuma, K., Aoki, S., and Nakazawa, T.: New technique for high-precision, simultaneous measurements of CH_4, N_2O and CO_2 concentrations; isotopic and elemental ratios of N_2, O_2 and Ar; and total air content in ice cores by wet extraction, Atmospheric Measurement Techniques, 13, 6703–6731, 2020.

Pedro, J. B., Jochum, M., Buizert, C., He, F., Barker, S., and Rasmussen, S. O.: Beyond the bipolar seesaw: Toward a process understanding of interhemispheric coupling, Quaternary. Sci. Rev., 192, 27–46, https://doi.org/10.1016/j.quascirev.2018.05.005, 2018.

Prather, M. J., Hsu, J., DeLuca, N. M., Jackman, C. H., Oman, L. D., Douglass, A. R., Fleming, E. L., Strahan, S. E., Steenrod, S. D., Søvde, O. A., Isaksen, I. S. A., Froidevaux, P., and Funke, B.: Measuring and modeling the lifetime of nitrous oxide including its variability, J. Geophys. Res.-Atmos., 120, 5693–5705, https://doi.org/10.1002/2015JD023267, 2015.

Rasmussen, S. O., Bigler, M., Blockley, S. P., Blunier, T., Buchardt, S. L., Clausen, H. B., Cvijanovic, I., Dahl-Jensen, D., Johnsen, S. J., Fischer, H., Gkinis, V., Guillevic, M., Hoek, W. Z., Lowe, J. J., Pedro, J. B., Popp, T., Seierstad, I. K., Steffensen, J. P., Svensson, A. M., Vallelonga, P., Vinther, B. M., Walker, M. J. C., Wheatley, J. J., and Winstrup, M.: A stratigraphic framework for abrupt climatic changes during the Last Glacial period based on three synchronized Greenland ice-core records: refining and extending the INTIMATE event stratigraphy, Quaternary. Sci. Rev., 106, 14–28, https://doi.org/10.1016/j.quascirev.2014.09.007, 2014.

Rhodes, R. H., Brook, E. J., Chiang, J. C. H., Blunier, T., Maselli, O. J., McConnell, J. R., Romanini, D., and Severinghaus, J. P.: Enhanced tropical methane production in response to iceberg discharge in the North Atlantic, Science, 348, 1016–1019, https://doi.org/10.1126/science.1262005, 2015.

Rhodes, R. H., Faïn, X., Brook, E. J., McConnell, J. R., Maselli, O. J., Sigl, M., Edwards, J., Buizert, C., Blunier, T., Chappellaz, J., and Freitag, J.: Local artifacts in ice core methane records caused by layered bubble trapping and in situ production: a multi–site investigation, Clim. Past, 12, 1061–1077, https://doi.org/10.5194/cp-12-1061-2016, 2016.

Rosen, J. L., Brook, E. J., Severinghaus, J. P., Blunier, T., Mitchell, L. E., Lee, J. E., Edwards, J. S., and Gkinis, V.: An ice core record of near-synchronous global climate changes at the Bølling transition, Nat. Geosci., 7, 459–463, https://doi.org/10.1038/ngeo2147, 2014.

Schilt, A., Baumgartner, M., Blunier, T., Schwander, J., Spahni, R., Fischer, H., and Stocker, T. F.: Glacial–interglacial and millennial-scale variations in the atmospheric nitrous oxide concentration during the last 800,000 years, Quaternary. Sci. Rev., 29, 182–192, https://doi.org/10.1016/j.quascirev.2009.03.011, 2010a.

Schilt, A., Baumgartner, M., Schwander, J., Buiron, D., Capron, E., Chappellaz, J., Loulergue, L., Schüpbach, S., Spahni, R., Fischer, H., and Stocker, T. F.: Atmospheric nitrous oxide during the last 140,000 years, Earth. Planet. Sc. Lett., 300, 33–43, https://doi.org/10.1016/j.epsl.2010.09.027, 2010b.

Schilt, A., Baumgartner, M., Eicher, O., Chappellaz, J., Schwander, J., Fischer, H., and Stocker, T. F.: The response of atmospheric nitrous oxide to climate variations during the last glacial period, Geophys. Res. Lett., 40, 1888–1893, https://doi.org/10.1002/grl.50380, 2013.

Schilt, A., Brook, E. J., Bauska, T. K., Baggenstos, D., Fischer, H., Joos, F., Petrenko, V. V., Schaefer, H., Schmitt, J., Severinghaus, J. P., Spahni, R., and Stocker, T. F.: Isotopic constraints on marine and terrestrial N_2O emissions during the last deglaciation, Nature, 516, 234–237, https://doi.org/10.1038/nature13971, 2014.

Schmitt, J., Seth, B., Bock, M., and Fischer, H.: Online technique for isotope and mixing ratios of CH_4, N_2O , Xe and mixing ratios of organic trace gases on a single ice core sample, Atmos. Meas. Tech., 7, 2645–2665, https://doi.org/10.5194/amt-7-2645-2014, 2014.

Schmittner, A. and Galbraith, E. D.: Glacial greenhouse-gas fluctuations controlled by ocean circulation changes, Nature, 456, 373–376, https://doi.org/10.1038/nature07531, 2008.

Skinner, L. C. and Shackleton, N. J.: Deconstructing Terminations I and II: revisiting the glacioeustatic paradigm based on deep-water temperature estimates, Quaternary. Sci. Rev., 25, 3312–3321, https://doi.org/10.1016/j.quascirev.2006.07.005, 2006.

Sowers, T.: N_2O record spanning the penultimate deglaciation from the Vostok ice core, J. Geophys. Res.-Atmos., 106, 31 903–31 914, https://doi.org/10.1126/science.1121235, 2001.

Spahni, R., Chappellaz, J., Stocker, T. F., Loulergue, L., Hausammann, G., Kawamura, K., Flückiger, J., Schwander, J., Raynaud, D., and Masson-Delmotte, V.: Atmospheric methane and nitrous oxide of the late Pleistocene from Antarctic ice cores, Science, 310, 1317–1321, https://doi.org/10.1126/science.1120132, 2005.

Stanford, J. D., Rohling, E. J., Hunter, S. E., Roberts, A. P., Rasmussen, S. O., Bard, E., McManus, J., and Fairbanks, R. G.: Timing of meltwater pulse 1a and climate responses to meltwater injections, Paleoceanography, 21, https://doi.org/10.1029/2006PA001340, 2006.

Stocker, T. F. and Johnsen, S. J.: A minimum thermodynamic model for the bipolar seesaw, Paleoceanography, 18, https://doi.org/10.1029/2003PA000920, 2003.

Tarasov, L. and Peltier, W. R.: Arctic freshwater forcing of the Younger Dryas cold reversal, Nature, 435, 662–665, https://doi.org/10.1038/nature03617, 2005.

Van Groenigen, K. J., Osenberg, C. W., and Hungate, B. A.: Increased soil emissions of potent greenhouse gases under increased atmospheric CO_2, Nature, 475, 214–216, https://doi.org/10.1038/nature10176, 2011.

Veres, D., Bazin, L., Landais, A., Toyé Mahamadou Kele, H., Lemieux-Dudon, B., Parrenin, F., Martinerie, P., Blayo, E., Blunier, T., Capron, E., Chappellaz, J., Rasmussen, S. O., Severi, M., Svensson, A. M., Vinther, B. M., and Wolff, E. W.: The Antarctic ice core chronology (AICC2012): an optimized multi–parameter and multi-site dating approach for the last 120 thousand years, Clim. Past, 9, 1733–1748, https://doi.org/10.5194/cp-9-1733-2013, 2013.

WAIS Divide Project Members: Precise interpolar phasing of abrupt climate change during the last ice age., Nature, 520, 661, https://doi.org/10.1038/nature14401, 2015.

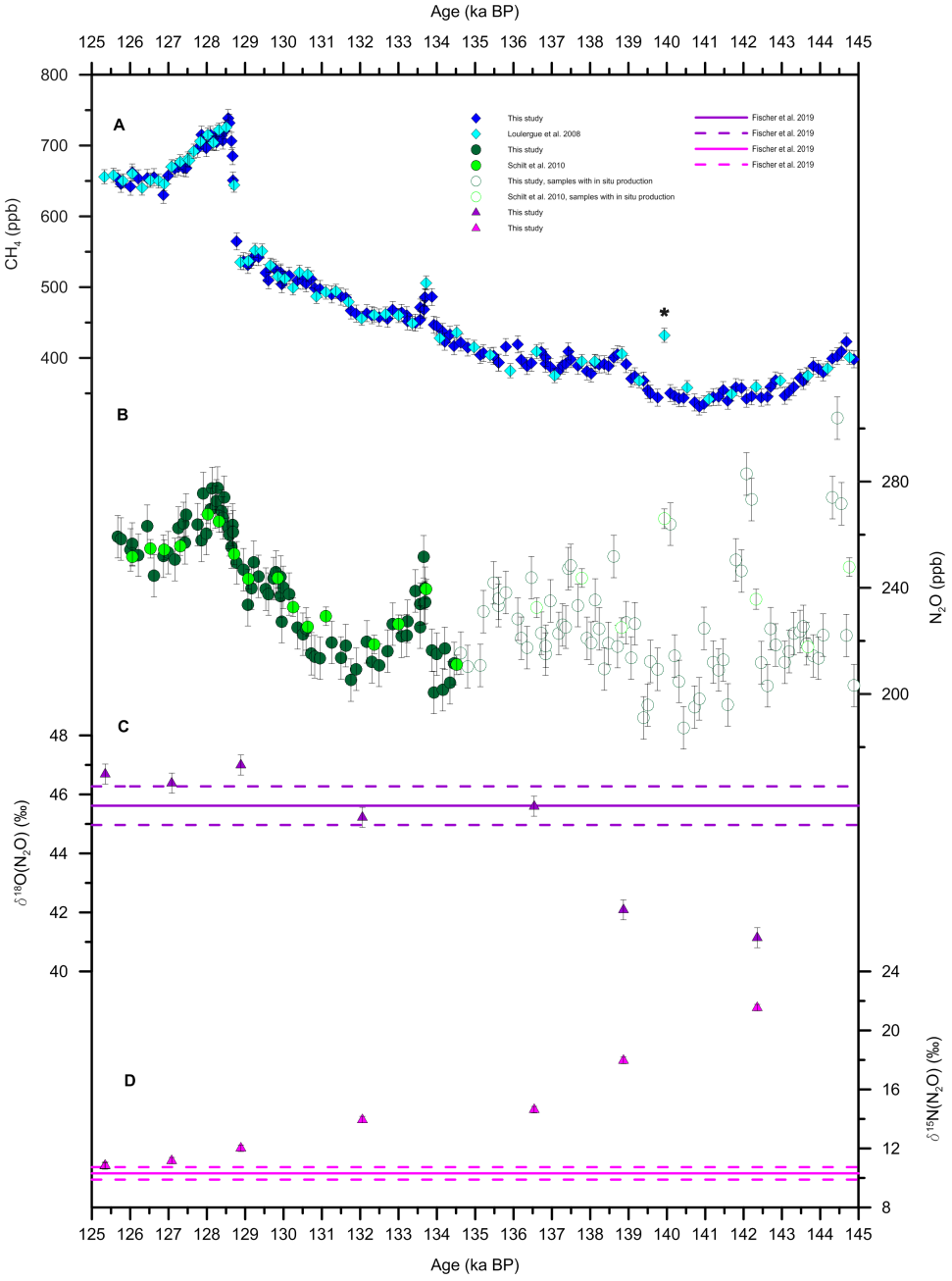

Figure 1. CH_4, N_2O, $\delta^{18}O(N_2O)$ and $\delta^{15}N(N_2O)$ records from the EDC ice core on the AICC2012 timescale (Bazin et al., 2013). The vertical bars represent the uncertainty of the measurements. ~~(A):~~ **A:** Composite CH_4 record with published data (light blue, Loulergue et al. (2008)) and new measurements (this study, dark blue) after offset correction. ~~(B):~~ The asterisk indicates the data point considered as an outlier. **B:** Composite N_2O record with published data (light green, Schilt et al. (2010a)) and new measurements (this study, dark green) after offset correction. The empty symbols illustrate the data points considered ~~as~~ affected by in situ production. ~~(C):~~ **C:** $\delta^{18}O(N_2O)$ record. For comparison, ~~a solid and a dashed lines are included, representing~~ the average (solid line) and standard deviation (dashed line, 1σ) ~~, respectively,~~ of ~~the isotopic values during~~ $\delta^{18}O(N_2O)$ over TI are included (Fischer et al., 2019). ~~(D):~~ **D:** $\delta^{15}N(N_2O)$ record. For comparison, ~~including~~ the average (solid line) and standard deviation (dashed ~~lines as in (C). (E):~~ ~~Rates of CH_4 change~~line, ~~calculated by differentiating splines (Enting, 1987) (cut-off period = 200 years~~1σ) ~~fitted through the composite record. (F):~~ ~~Rates~~ of ~~N_2O change, for the section unbiased by artifacts, calculated as in (E)~~$\delta^{15}N(N_2O)$ over TI are included (Fischer et al., 2019).

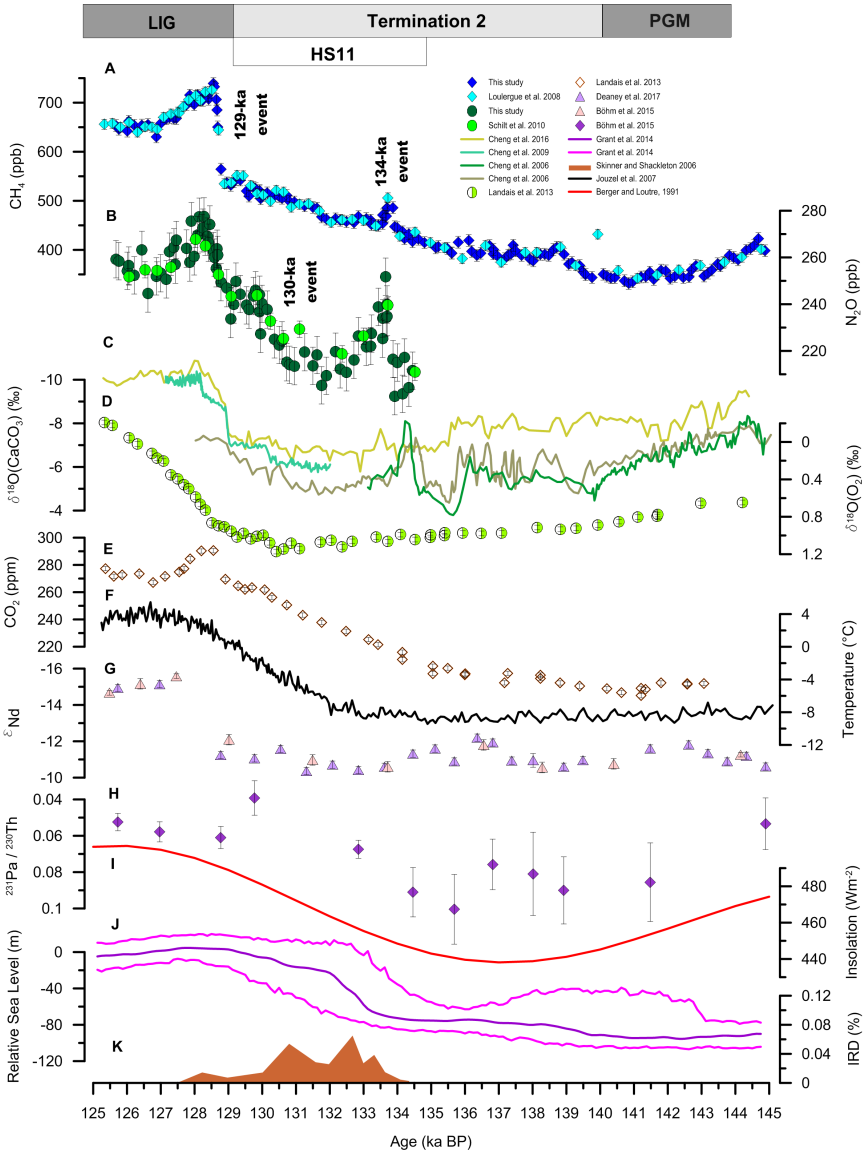

Figure 2. Evolution of the CH_4 and N_2O concentrations combined with complementary climate proxies during TII. ~~The shadings delineate the climatic events as described in Fig.2. The individual records are plotted on their own timescales, with the vertical bars representing the uncertainty of the measurements as reported in the references.~~The boxes delineate the climate periods mentioned in the text: the Penultimate Glacial Maximum (PGM), Heinrich Stadial 11 (HS11, delineation according to Marino et al. (2015)). ~~(A)~~**A**: Composite CH_4 record ~~(this study, as in Fig.1)~~. ~~(B)~~**B**: Composite N_2O record ~~(this study, as in Fig.1)~~. ~~(C)~~**C**: Speleothems $\delta^{18}O(CaCO_3)$ records: Sanbao SB25 (light green) (Cheng et al., 2009), Hulu Cave MSX (khaki) (Cheng et al., 2006), Hulu cave MSP (dark green) (Cheng et al., 2006), and Sanbao-Dongge composite (pale yellow) (Cheng et al., 2016). ~~Each speleothem record is plotted on its individual radiometric timescale.~~ ~~(D)~~**D**: $\delta^{18}O(O_2)$ from EDC on the AICC2012 timescale (Landais et al., 2013). ~~(E)~~**E**: CO_2 from EDC on the AICC2012 timescale (Landais et al., 2013). ~~(F)~~**F**: ~~$\delta^{15}N(N_2O)$ from the EDC ice core on the AICC2012 timescale (Landais et al., 2013).~~Antarctic surface temperature (relative to the last millennium) from EDC on the AICC2012 timescale (Jouzel et al., 2007) . ~~(G)~~**G**: Composite ε_{Nd} from the sediment core ODP Site 1063 (Deaney et al., 2017), including data points from Böhm et al. (2015) (purple) and new measurements from Deaney et al. (2017) (pale pink), on the timescale of Deaney et al. (2017). ~~(H)~~**H**: ^{231}Pa / ^{230}Th record from the sediment core ODP Site 1063 (Böhm et al., 2015), on the timescale of Deaney et al. (2017). ~~(I)~~**I**: ~~Relative sea level stand from the Red Sea synchronized on a radiometric timescale, including the maximum probability curve (purple) and its 95% confidence interval (magenta)~~Mean summer (June to August) insolation at 40°N (Berger and Loutre, 1991) . ~~(J)~~**J**: ~~Ice-rafted debris (IRD) from Skinner and Shackleton (2006) on the radiometric timescale of Marino et al. (2015).~~ Relative sea level stand from the Red Sea synchronized on a radiometric timescale, including the maximum probability curve (purple) and its 95% confidence interval (magenta) (Grant et al., 2014). **K** : Ice-rafted debris (IRD) from Skinner and Shackleton (2006) on the radiometric timescale of Marino et al. (2015).

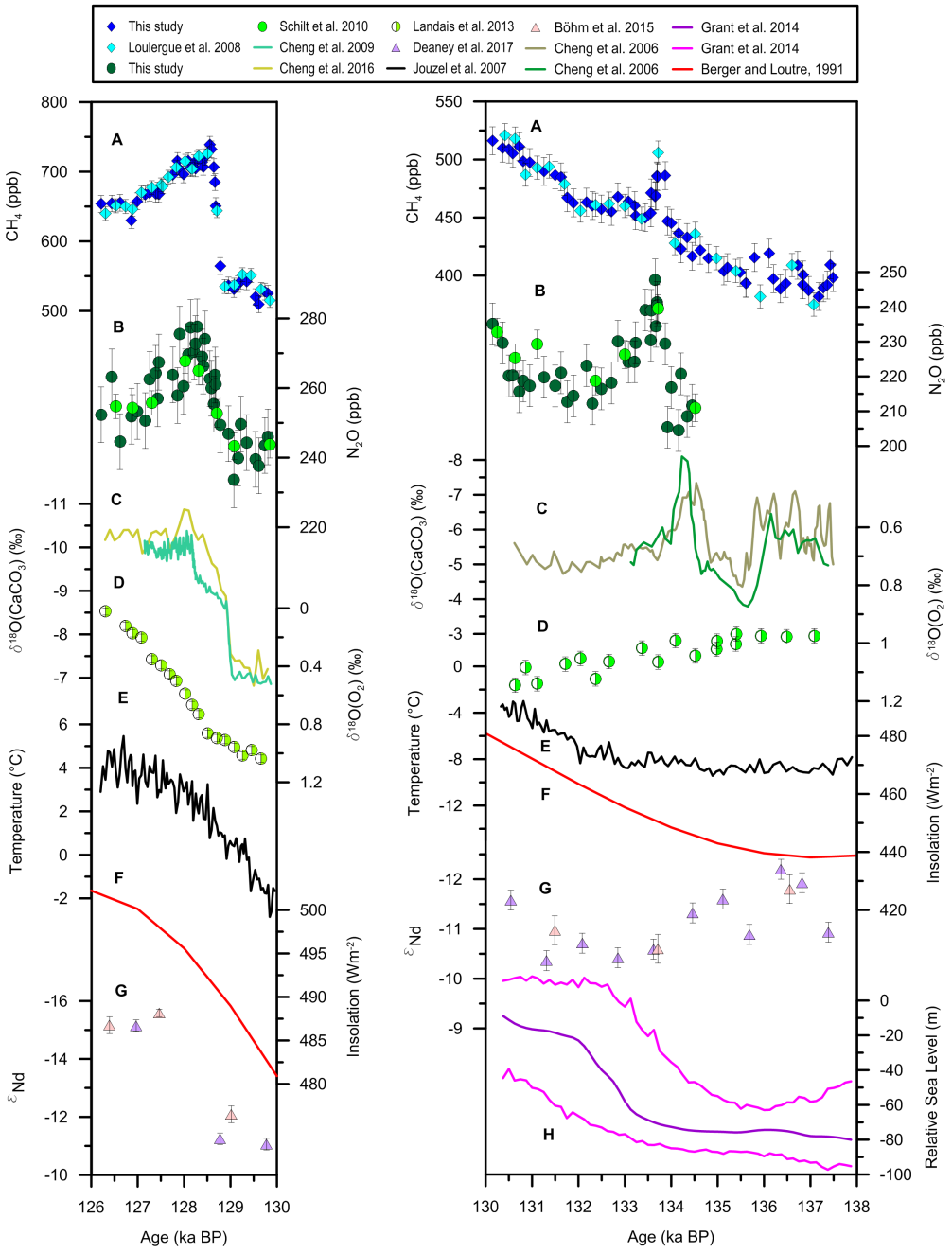

Figure 3. Details of the 128~~9~~(left panel) ~~, 130.5 (left panel)~~and 134-ka events (right panel) ~~for CH_4 (A), N_2O (B), and key climate proxies (from (C) onwards), symbols as described in Fig. 3.~~**A**: Composite CH_4 record. **B**: Composite N_2O record. **C**: Speleothems $\delta^{18}O(CaCO_3)$ records: Sanbao SB25 (light green) (Cheng et al., 2009), Hulu Cave MSX (khaki) (Cheng et al., 2006), Hulu cave MSP (dark green) (Cheng et al., 2006) , and Sanbao-Dongge composite (pale yellow) (Cheng et al., 2016). **D**: $\delta^{18}O(O_2)$ from EDC on the AICC2012 timescale (Landais et al., 2013). **E**: Antarctic surface temperature (relative to the last millennium) from EDC on the AICC2012 timescale (Jouzel et al., 2007). **F**: Mean summer (June to August) insolation at 40°N (Berger and Loutre, 1991). **G**: Composite ε_{Nd} from the sediment core ODP Site 1063 (Deaney et al., 2017), including data points from Böhm et al. (2015) (purple) and new measurements from Deaney et al. (2017) (pale pink), on the timescale of Deaney et al. (2017). **H**: Relative sea level stand from the Red Sea synchronized on a radiometric timescale, including the maximum probability curve (purple) and its 95% confidence interval (magenta) (Grant et al., 2014).

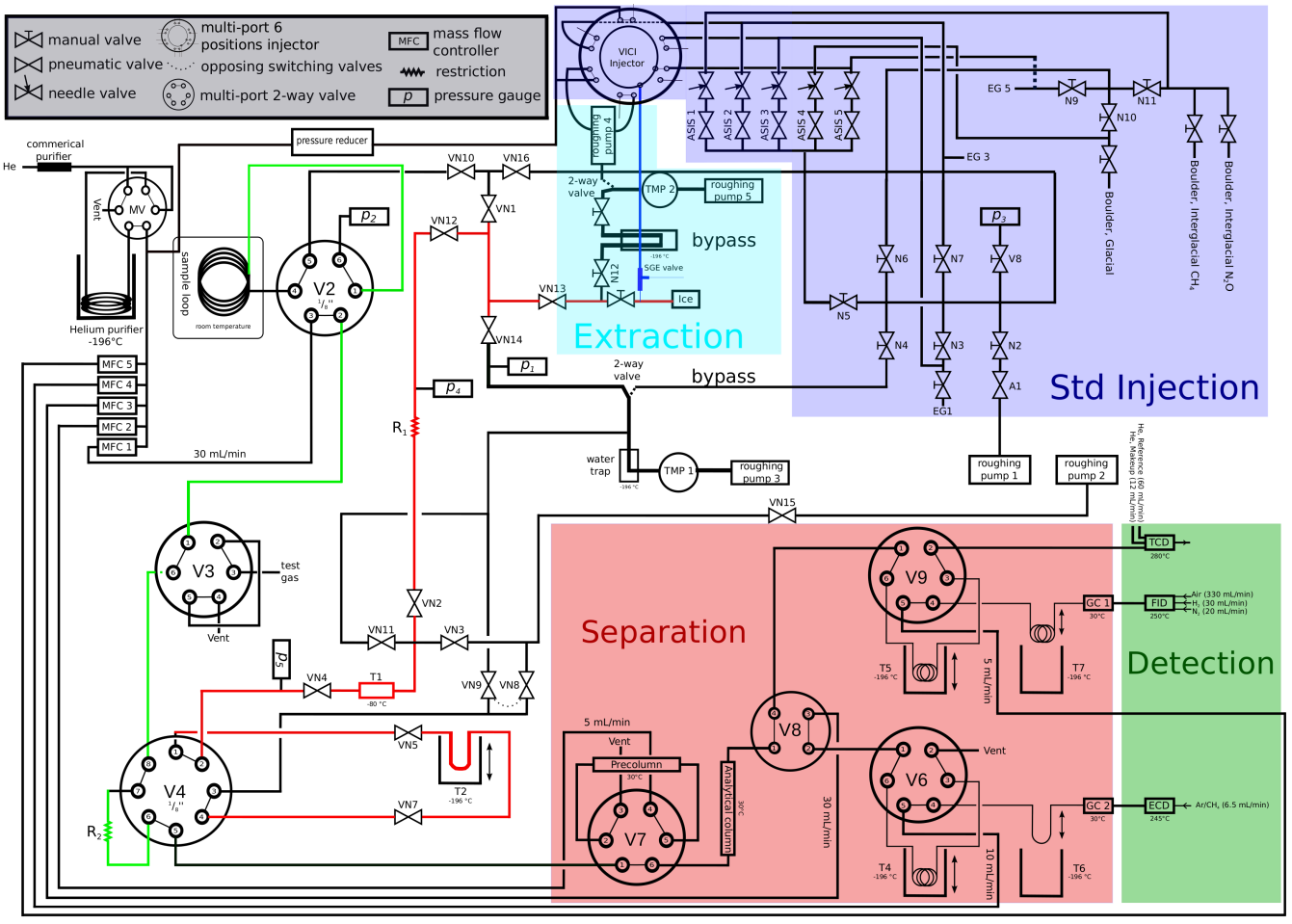

Figure 4. Flow scheme of the CH_4 and N_2O measurement system. The red, green and blue paths highlight the Ice Line (IL), Continuous-Flow Line (CFL) and Standard Over Ice Line (SOIL), respectively. Colored boxes display the different functional units of the system discussed in Appendix A.

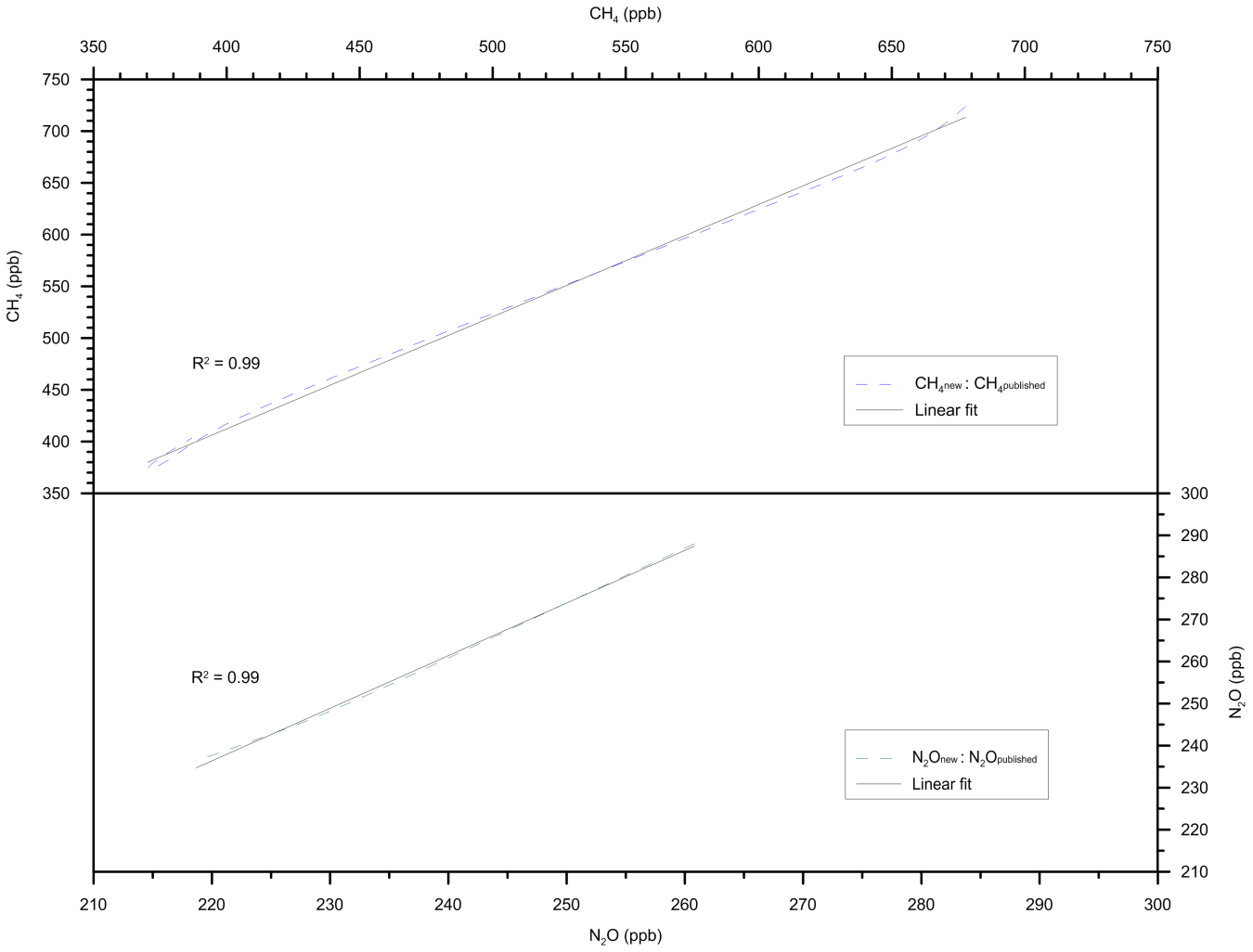

Figure 5. Offsets between new and published CH_4 and N_2O EDC records. Dashed lines show the new measurements plotted against the published ones (data are from the spline approximations introduced in Appendix B). Solid lines are linear fits through these data.

Table 1. Characteristics of the events observed at ∼134, ∼129 and ∼130 ka BP. The indications *up* and *down* in the first column refer to the ascending and descending limbs of the 134-ka event, respectively. The columns *start* and *end* indicate the starting and end points of the events (rounded to the hundred). The columns $C_{initial}$ and C_{final} indicate the concentrations (rounded to the ten) in the years preceding and following the events, respectively. The rates of change are average values over the time period comprised between the start and end points of the events. Rates of change are calculated from spline approximations (cut-off period = 200 years) computed according to Enting (1987) with the same routine as Beck et al. (2018).

Event	**Start (ka BP)**	**End (ka BP)**	**$C_{initial}$ (ppb)**	**C_{final} (ppb)**	**Rate of change (ppb per century)**
134 (CH_4, up)	134.0	133.8	440	510	35
134 (CH_4, down)	133.8	133.4	510	450	-15
134 (N_2O, up)	133.9	133.6	210	240	10
134 (N_2O, down)	133.6	132.6	240	210	-3
130 (N_2O)	130.7	130	220	240	3
129 (CH_4)	128.9	128.6	530	730	65
129 (N_2O)	129	128.1	240	270	3